11-1-2018

Wolfe Creek Crater: A continuous sediment fill in the Australian Arid Zone records changes in monsoon strength through the Late Quaternary

Gifford H. Miller

John W. Magee

Marilyn L. Fogel

Matthew J. Wooller

Paul P. Hesse

See next page for additional authors

Recommended Citation

Miller, G.H., Magee, J., Fogel, M., Wooller, M., Hesse, P., Spooner, N., Johnson, B., Wallis, L., (2018) Wolfe Creek Crater: A continuous sediment fill in the Australian Arid Zone records changes in monsoon strength through the late Quaternary. Quaternary Science Reviews, 199, 108-125. https://doi.org/10.1016/j.quascirev.2018.07.019

Authors
Gifford H. Miller, John W. Magee, Marilyn L. Fogel, Matthew J. Wooller, Paul P. Hesse, Nigel A. Spooner, Beverly J. Johnson, and Lynley Wallis

Wolfe Creek Crater: A continuous sediment fill in the Australian Arid Zone records changes in monsoon strength through the Late Quaternary

Gifford H. Miller[1], John W. Magee[2], Marilyn L. Fogel[3], Matthew J. Wooller[4], Paul P. Hesse[5], Nigel A. Spooner[6], Beverly J. Johnson[7], and Lynley Wallis[8]

[1] *INSTAAR and Department of Geological Sciences, University of Colorado,* Boulder CO 80309 USA
[2] *Research School of Earth Sciences, Australian National University, Acton ACT 0200 (retired)*
[3] *Dept. of Earth Science, University of California Riverside, Riverside, CA, USA.*
[4] *Water and Environmental Research Center, Institute of Northern Engineering, University of Alaska Fairbanks, Fairbanks, Alaska, USA and Alaska Stable Isotope Facility, School of Fisheries and Ocean Sciences, University of Alaska Fairbanks, Fairbanks, Alaska, USA.*
[5] *Department of Environmental Sciences, Macquarie University, Sydney, NSW, Australia.*
[6] *Institute for Photonics & Advanced Sensing and School of Physical Sciences, University of Adelaide, Adelaide, 5005, Australia, and Defense Science & Technology Group, Edinburgh 5111, SA, Australia*
[7] *Dept. of Geology, Bates College, Lewiston, ME 04240*
[8] *Nulungu Research Institute, University of Notre Dame Australia, PO Box 2287, Broome WA, 6725, Australia*

Abstract

A bolide that impacted NW Australia during the Late Quaternary left a circular depression more than 100 m deep and nearly a kilometer in diameter, with a crater rim ~30 m above the regional terrain. The resultant crater is a window into the regional water table. The surface of the contemporary central pan is 25 m below the adjacent terrain, coincident with the late Holocene regional water table modified by local evaporative processes. Shielded from aeolian deflation by the crater rim, the central depression has slowly filled with dust, sand, and chemical precipitates, estimated to be 20 to 100 m thick based on geophysical surveys, one of the few continuous depocenters known in the Australian Arid Zone. The nature of the crater's sediment fill is controlled by interactions between the depth of the water table, primarily in response to changes in summer monsoon rain, changes in the delivery of sand and dust to the crater by the prevailing easterly winds, and the level of the sedimentary fill surface. We describe and interpret the upper 10 m of sediment fill recovered from the central pan. Optically Stimulated Luminescence (OSL) and ^{14}C dates constrain an age model indicating the sediments span the past ~60 ka. The lowest 3 m Marine Isotope Stage (MIS) 3, consist of clayey sand deposited in perennial water. The water table dropped rapidly ~35 ka and remained more than 7 m below the late Holocene level through most of MIS 2, and 2 m of sandy clay was deposited on a dry crater floor, confirming a dry and dusty Last Glacial Maximum (LGM) climate. By 14 ka a rising water table intersected the crater surface, modifying the upper 50 cm of LGM sediment, and syndepositionally modifying another 60 cm of subsequent sandy clay deposition. Aeolian sediment delivery effectively ceased ~13 ka, and the upper 4.8 m is a gypsum-dominated precipitate, which initially accumulated

rapidly, before equilibrating with the late Holocene water table shortly after 6 ka. Lacustrine carbonate encrustations on rocks at the base of the crater wall dated >40 ka document a time when regional groundwater maintained a water body in the crater 3.5 to 4.5 m above the central pan. The crater wall deflected the prevailing easterly winds, creating a horseshoe-dune extending westerly on both sides of the crater. An augered hole through the northern dune revealed 10 m of sediment overlying ferricrete. The lowest meter is a mixture of broken ferricrete and sand that we interpret to be debris from bolide impact. Three OSL dates through the dune project an age for debris-dune contact of 120 ± 10 ka. Changes in physical properties and bulk sediment $\delta^{13}C$ through the 9 m of aeolian sediment indicate the lowest 1.8 m was deposited during MIS 5 (120 - 85 ka), under a uniformly wetter climate than present. The overlying 4.3 m of sediment was deposited between 85 and 14 ka (MIS 4, 3, 2) and exhibits transitional characteristics between the lower unit and the upper 3.8 of sand, which was deposited primarily during the Holocene. Large changes in the regional water table occurred over the past 60 ka, including an LGM water table persistently ≥7 m lower than late Holocene levels, and 3.5 to 4.5 m higher prior to 40 ka, plausibly late in MIS 5, indicative of a stronger Australian summer monsoon than at any time subsequently. Age models and sediment properties from the two sedimentary records indicate the crater was formed >60 ka and most likely ~120 ka, more recently than earlier estimates.

1. Introduction

Continuous records of Quaternary environmental change for Australia are restricted to the better-watered peripheral reaches of the continent, and from terrestrial proxies preserved in marine sediment on the adjacent shelves (van der Kaars and DeDeckker, 2002; Hesse et al., 2004, van der Kaars et al., 2006). Important, but discontinuous records come from the infilling and aeolian deflation of playa lakes across the arid zone. Of these, the record from Kati Thanda-Lake Eyre (KT-LE), the terminal depocenter of the ~1.2 x 10^6 km^2 Lake Eyre Basin, is the most complete. With its catchment in monsoon-watered northern Australia, KT-LE has served as an integrator of monsoon strength on millennial timescales ((Magee *et al.*, 2004; Cohen *et al.*, 2012). Reconstructions of the KT-LE lake level show a perennial lake during Marine Isotope Stage 5 (MIS 5), and intermittently until ca. 50 ka[1], followed by desiccation, with only a slight increase in wetness during the early Holocene. The lack of a strong increase in monsoon rains during the Holocene, when regional conditions (i.e., high sea level, high sea-surface temperatures, strong land-sea pressure gradients) were favorable for strong monsoon circulation, coupled with compelling evidence for a perennial water body in KT-LE as recently as 50 ka when regional conditions were less favorable, remains a climate enigma (Johnson et al., 1999; Miller et al., 2016).

Several other large salt lakes in the monsoon-watered northern regions of the arid zone contain evidence of former perennial water bodies in the form of shorelines and wave-eroded dune systems: Lake Buchanan (Chivas et al., 1986), Lake Woods (Bowler et al., 1998), Lake Gregory (Bowler et al, 2001), Lake Lewis (English et al., 2001), Lake Amadeus (Chen et al., 2007). Although dating former high water levels remains challenging, none carried perennial water within radiocarbon time, the past 40 ka. Most of these systems

[1] ka: thousands of years before present; calibrated when based on radiocarbon dates.

experienced extensive deflation of playa sediment during arid phases, so fail to provide continuous records of climate and environmental change on Quaternary timescales.

In previous work we developed a 130 ka record of stable carbon and oxygen isotope variations in eggshell of the giant flightless bird *Dromaius* (emu) from five different regions across the southern reaches of the arid zone (Miller et al., 2016). These records reveal an abrupt change in *Dromaius* dietary sources ~50 ka, that reflects a major reduction of C_4 summer-wet grasses available for the birds to eat. One plausible explanation for the loss of C_4 grass in *Dromaius* diet is a persistent reduction of summer rain reaching the continental interior after 50 ka, including the Holocene, consistent with the KT-LE lake-level reconstructions. We sought to test this interpretation by securing a continuous Late Quaternary record of rainfall from within monsoonal northern Australia. Wolfe Creek Crater appeared, in principle, to offer the possibility of a continuous, long (>100 ka), sedimentary record within the monsoonal north of the continent.

2. Wolfe[2] Creek Crater

Wolfe Creek Crater (WCC, Fig. 1: -19.17; 127.80), was formed in gently folded Devonian quartz sandstone, capped by a thin ferricrete of probable Miocene age (Hawke, 2003), and patchy longitudinal quartz sand dunes of Quaternary age (Fitzsimmons et al., 2012). The local Djaru people are the traditional owners of the crater, which they call Kandimalal. The crater has long been known to the Djaru and it features prominently in their beliefs. The crater was first reported in print by Reeves and Chalmers (1948) who initially postulated an explosive volcanic origin, but subsequently accepted a meteoritic impact as the most likely explanation. An Australian Geographic Society expedition visited the crater in 1948 and shortly thereafter Guppy and Matheson (1950) carried out detailed geological investigations. Both teams attributed the crater to a meteoritic impact based on the morphological similarity to known meteoritic craters, structural features in accordance with those predicted theoretically to be associated with impact craters, and weathered fragments of iron-oxide-rich metallic material that contained 1.9% nickel oxide, far in excess of that expected in terrestrial rocks. Further work on the weathered fragments by Cassidy (1954) and La Paz (1954) reinforced a meteoritic origin.

The meteorite impact left a nearly circular crater in the relatively flat terrain of NW Australia, averaging 885 m in diameter. The crater wall, which extends ~30 m above the surrounding landscape, is composed of bedrock blocks and dune sand thrown up by the impact. The central depression has been slowly infilled by dust, aeolian sand, and chemical precipitates. The crater's central pan, currently ~25 m below the adjacent landscape and ~265 m across, is flat, confirming it to be a groundwater controlled surface. From the pan edge, the landscape slopes upward to the crater wall, more steeply on the eastern side than on the western side. When visited by us in 1999 and 2001 the water table was within a meter of the pan floor, but on an earlier visit in 1979 by one of us (JWM), after prolonged drought, the water table was not visible and a number of shallow (~1 m) sink holes and short solution

[2] The crater is near an ephemeral creek, initially written "Wolf Creek", but later changed to "Wolfe Creek", when it was learned that the person for whom the creek was named spelled their name with an "e". Both names have been used for the crater, but "Wolfe" is now the official name.

cavities of unknown extent and depth had developed in massive gypcrete on the pan floor.

The fresh appearance and steep crater walls suggest a relatively young age for the impact event. A preliminary estimate of ~300 ka for the formation of the crater was provided by Shoemaker et al. (1990), based on the ratios of cosmogenic nuclides $^{36}Cl/^{10}Be$ and $^{41}Ca/^{36}Cl$ in fresh meteorite fragments found some distance from the crater. They also report exposure ages from cosmogenic ^{10}Be and ^{26}Al in quartzite boulders collected on the crater wall of ~30 ka. The younger exposure ages were interpreted to indicate ~6 m of rock erosion since the rim stabilized.

2.1 Post-impact sediment fill Meteorite impact craters experience an initial infill of impact rubble and breccia that rest on a zone of fractured rock. Once the crater rim has stabilized, the depression begins to fill with sediment and chemical precipitates, all of relatively low density. Based on gravity anomalies, Fudali (1979) suggested the initial Wolfe Creek Crater was 275 m deep, rapidly backfilled with 180 m of impact rubble, that was overlain by 95 m of sediment fill, slightly greater than estimates from morphometric relations (Grieve and Pilkington, 1996). Based on an airborne geophysical survey, Hawke (2003) supported the greater depth estimates and concluded the impactor was an iron–nickel meteorite ~50 m in diameter, but noted the strong dependency of crater depth calculations on density estimates for the crater fill. In contrast, O'Neill and Heine (2005) estimated an impactor 15 m in diameter, with ~100 m of post-impact breccia fill, overlain by another ~20 m of aeolian and slopewash sediment and chemical precipitates.

The combination of plausibly 300 ka of undisturbed sediment, amounting to at least 20 m thickness, and possibly considerably more, situated well within the influence of the Australian Summer Monsoon (Fig. 1), offered a promising target to reconstruct the evolution of monsoon rainfall through the Late Quaternary.

2.2 Modern climate, vegetation, and groundwater The regional climate is monsoonal. Climate data are available from two nearby weather stations with multi-decadal continuous precipitation data: Halls Creek, 100 km north of the crater, with a 67-year record (1944-2017), and a longer (1889-2017), but less continuous record from Sturt Creek Station, 40 km east of the crater (Fig. 1). On average, 80% of the annual rainfall is received between December and March at both stations, with an average annual rainfall at Halls Creek of 580 mm, whereas Sturt Creek Station receives slightly less, 430 mm, for the same interval. Rainfall at the crater would have the same seasonal pattern, with an interpolated average annual rainfall of ~500 mm. Monthly temperature maxima range from 27 to 38°C and monthly minima range from to 13 to 24°C at Halls Creek. Evaporative water loss from the site is highest between September and January, with an annual average point potential evapotranspiration of 3200 mm, far in excess of the average annual rainfall (~500 mm).

With a catchment of only 0.6 km^2 and high potential evaporation, local rainfall is unable to sustain a lake within the crater. Rather, the crater water table is controlled by the regional groundwater table, reduced by within-crater evaporative pumping (Macumber, 1992). The response of regional groundwater to changes in rainfall depends on the size of the groundwater basin, aquifer confinement and transmissivity, upbasin head, downbasin throughflow efficiency, discharge losses to local creeks, and other variables, all of which are

poorly known. However, our water-table-difference observations are evidence that the crater water table is sensitive to changes in rainfall on decadal timescales. Such changes reflect the sensitive balance between the depth of a relatively small groundwater window into a large regional water table. The within-crater water table will fluctuate on Quaternary timescales in response to changes in the strength of the summer monsoon, with resultant morphological and sedimentological consequences.

Wooller et al. (2005) describe the vegetation within and around the crater. Cyperaceae and herbaceous plants of the genera *Atriplex* and *Flaveria* use C_4 photosynthesis, whereas all tree genera from the crater (*Acacia*, *Crotalaria*, *Dolichandrone*, *Eucalyptus*, *Hakea*, *Melaleuca*, and Trichodesma) use C_3 photosynthesis, as do the herbs *Newcastelia* and *Ptilotus*. The C_3 plants within the crater have an average $\delta^{13}C$ value of -26.5 ± 0.6‰, whereas the C_4 plants average -12.0 ± 1.6‰ (Wooller et al., 2005). Carbon preserved in surface sediment collected across the crater had intermediate $\delta^{13}C$ values, ranging from -15 to -20‰ representing the mix of C_3 and C_4 isotopic end members observed across the modern crater floor.

2.3. Crater wall alters regional dune field The local terrain around the crater is a gently undulating bedrock surface dipping to the south at ~1 m km^{-1}. The landscape is mantled by ENE-WSW trending longitudinal dunes aligned with the regional wind rose (Fig. 3). Spaced ~1 km apart, with basal widths of ~100 m, and we expect they were in approximately the same position at the time of impact (Hesse, 2011). A thin ferricrete layer dominates the inter-dune landscape with patchy, thin sandy sediment locally overlying the ferricrete. The bolide impact occurred at the crest of one of the longitudinal dunes (Fig. 4). The formation of the crater wall at the dune crest became an obstacle to wind-transported sediment. Consequent deflection of easterly winds by the crater wall resulted in the creation of a new horseshoe-shaped dune wrapping around the crater (Fig. 4) similar to those described by (Mchone et al. (2002), and a sand ramp built up against the eastern crater rim.

2.4 Field campaigns In 1969 the crater became the Wolfe Creek Meteorite Crater National Park, overseen by the Western Australia Department of Conservation and Land Management (CALM). Both the Traditional Owners of the crater in nearby Billiluna and CALM gave permission for and assistance with the sampling we undertook. The crater was first visited by a member of our team (JWM) in 1979, who recovered a bulk sample from the wall of a sinkhole in the central pan, and a sample of crater wall rock, that were subjected to mineralogical analyses, reported in Section 6.

Our 1999 field goal was to recover a stratigraphic sequence of sediment samples from the central pan at about 10 cm intervals to evaluate whether the crater fill was suitable for a more ambitious effort to recover a long, continuous sediment core. We utilized a motorized augering system (dormersoilsamples.com), consisting of a stainless steel "Jarret"-style auger head, 10 cm in diameter, attached to a string of threaded aluminum rods, 4 cm x 150 cm, and rotated using a gasoline-powered hydraulic drive unit (Drillmite), supplied by Dormer (Fig. 5). We recovered ~10 m of sediment (WCC99-04) the limit of our extension rods. Augering has advantages over coring the crater fill, as the upper 5 m of sediment includes thick layers

of indurated gypsum, that an auger can slowly erode, but when sampled by hydraulic coring results in bent core tubes, or intractable sediment fill. The disadvantage of augering is that the sediment fabric is disturbed. Although contamination by younger, overlying sediment is possible, careful sampling can limit this effect. Each interval sampled consisted of a drive of ~10 cm. Although there is always some sediment infill from the previous sample or hole wall scrapings, the lowermost 5 cm are intact. After removing sediment in the blades of the auger, we sample the sediment in lowermost 3 cm of the auger barrel after each drive. We ascribe each sample to represent a bulk sample at a depth midway between the start and completion levels of each drive.

Initial analyses on the central crater samples indicated a stratified sediment fill that very likely extended continuously back in time tens of thousands of years, leading to a concerted effort to deliver a hydraulic coring rig to the center of the crater to recover a continuous core several tens of meters in length. A Jacro 105 petrol-powered hydraulic coring unit was trailered to the crater rim, and subsequently delivered to the crater floor via flying fox zip line and transported to the center of the pan, where it was positioned within 10 m of WCC99-04. Coring through the gypsum units with stainless-steel core barrels proved unsuccessful, due to the indurated gypsum. Instead, we drilled through 5 meters of gypsum-dominated sediment and attempted to core through the underlying loose sand. However, wet sand between 5.0 and 5.8 m depth lacked sufficient fine sediment to be retained in the core barrels. At 5.8 m depth the drilling encountered red sandy clay, which we successfully recovered in a 52 cm long core. Subsequently, 10 m of dune sand was sampled by augering from the north arm of the horseshoe dune (01WCC-13), and additional auger holes and hydraulic coring was completed through the sand ramp east of the crater rim.

3. Analytical Methods

3.1 Optically stimulated luminescence (OSL) Sampling for OSL dating was accomplished in the crater's central pan at 01WCC-02 using the Jacro 105 coring rig with a 52 cm long by 6.2 cm diameter stainless steel tube attached to the drill stem and driven into the sediment, then sealed by light-proof plastic caps on recovery. OSL sampling of dune sand outside the crater was undertaking after collecting a continuous series of sediment samples through the 10 m of sediment (01WCC-13). A parallel hole (01WCC-14), one meter from the primary hole was augered for OSL samples, targeted at specific depths based on observations of sediment recovered from 01WCC-13. When the designated sampling depth was reached, a special hole shaver (Fig. 5) developed for us by Dormer was used to provide a clean, flat surface. A 23 cm long, 62 mm diameter stainless steel tube was attached to a stainless steel drive adapter at the end of aluminum extension rods. A steel anvil was fixed to the drill stem protruding from the ground and a small sledgehammer was used to drive the OSL sample tube into the sediment until 20 cm of sediment penetration was accomplished (3 cm of the core barrel was occupied by the sampler head). The tube was sealed and capped on recovery; five levels were sampled for OSL dating in this manner.

The dated sites are well bleached aeolian sediment lacking any visible evidence of post-depositional bioturbation or other mixing. Bulk sediment from the 8 cm depth used for dating was analyzed for U, Th and K concentrations, which were measured by neutron

activation analysis and delayed neutron activation (NAA/DNA); K was calculated from measurements of K_2O by x-ray fluorescence (XRF). Radioisotope activities for U, Th, and K were also measured by high-resolution gamma spectrometry and subsequently converted to concentrations; these data confirmed secular equilibrium in the U and Th decay chains. Cosmic ray dose rates were calculated following Prescott and Hutton (1994), making allowance for site altitude, geomagnetic latitude and time-averaged thickness of sediment overburden. Alpha-particle irradiation from radioisotopes within the etched quartz grains was assumed to be 10% of the external activity, and the efficiency with which alpha-particle irradiation induced OSL (*a*) was assumed to be 0.04 ± 0.01. Long-term water content was estimated as described in section 6.2.

In the laboratory, 90-125 μm quartz grains were isolated from each sediment sample under low-intensity red and orange light. OSL measurements were performed on approximately 5 to 6 mg of etched quartz attached by silicone oil to the central 7 mm diameter of each of 128 stainless steel discs. The OSL signal was measured on an Elsec Type 9010 automated reader with 500 ± 80 nm stimulation, and UV emissions detected by an EMI 9235QA photomultiplier tube optically filtered by one UG 11 and one U-340 filter and P determined by the "Australian slide" using a linear plus single saturating exponential fit (scale factor = 1.00). More complete details are in Spooner et al. (2001). The advantage of multiple-grain OSL over single-grain OSL for these stratified low-dose-rate sediments is that the use of many grains effectively eliminates small-scale dose heterogeneity by averaging out the slight grain-to-grain differences in beta dose.

3.2 Radiocarbon All radiocarbon dates were prepared at the INSTAAR radiocarbon laboratory (NSRL: http://instaar.colorado.edu/research/labs-groups/laboratory-for-ams-radiocarbon-preparation-and-research/). Carbonate samples were given a light (oogonia) or extensive (lacustrine carbonates) acid leach, after which carbon was released by dissolving the remaining mass in phosphoric acid. Purified CO_2 was converted to graphite and measured at the W.M. Keck Carbon Cycle Accelerator Mass Spectrometry Laboratory at the University of California Irvine. Radiocarbon dates were calibrated with CALIB 7.1 using SHCal13 (Reimer et al., 2013); they are reported as conventional radiocarbon ages ±1σ, and as calibrated median ages with ±1σ ranges, and expressed as calibrated years before present.

3.3 Magnetic susceptibility (MS) Bulk sediment was transferred into 1-cm3 tubes. Sediment mass was calculated and MS was measured on a Bartington Magnetic Susceptibility Meter. Mass MS was measured on 109 samples through the 9.8 m augered hole in the central pan (99WCC-04), and in 105 samples from the dune core north of the crater. Mass MS was also measured in numerous surface samples within and around the crater.

3.4 Sedimentary organic matter An aliquot of augered sediment (12 to 16 mg) from each level was weighed into a tin capsule, which was introduced into an elemental analyzer (CE Instruments, NA 2500 series) at the Carnegie Institution of Washington's Geophysical Laboratory. Purified combustion gases were separated in a gas chromatographic column prior

to entering a Finnigan Conflo II interface and the stable isotope ratio mass spectrometer (Finnigan MAT, Delta-plus XL). The results are presented in standard delta notation (i.e. $\delta^{13}C$ values). Acetanilide (C_8H_9NO) was analyzed (every tenth sample) as a check on the analytical precision and accuracy throughout the analyses, which was ±0.3‰ for $\delta^{13}C$ values and ±5% of the %C value. A two end-member mixing model was used to calculate the proportion of C_3 and C_4 plants contributing to the bulk sediment $\delta^{13}C$, assuming the $\delta^{13}C$ value of C_3 □□□□□□ is -26.5‰ and for C_4 plants the $\delta^{13}C$ value is -11.5‰, the average $\delta^{13}C$ values of C_3 and C_4 plants within the crater (Wooller et al., 2005). The model assumes carbon preserved in sediment is incorporated without isotopic fractionation and minimal post-depositional translocation of carbon.

3.5 Hygroscopic moisture The difference in weight between air-dried sediment and oven-dried (15 hours at 105°C) sediment is reported as weight-percent moisture. Gypsum, hydrated calcium sulfate ($CaSO_4 \bullet 2H_2O$), is stable below 45°C, but is rapidly converted to bassanite at 105°C, liberating 1.5 water molecules. This release dominates the changes in hygroscopic moisture through WCC99-04.

3.6 Sediment properties Grain size was determined using a Malvern Mastersizer 3000 laser diffraction system and Hydro LV, measuring size ranges between 0.01-3500 μm. Quantitative (wt.%) data (qXRD) were determined on the <2 mm sediment fraction for nine levels from WCC99-04 using the method described by Eberl (2003). The samples were measured on a Siemens D5000 XRD between 5 and 65 two-theta at a 0.02 two-theta step with a two second count. The counts were imported into the Excel macro program RockJock v.6 (Eberl 2003), with 124 standard patterns, and the degree-of-fit (DOF is the minimum absolute difference) between a calculated and an observed pattern. Major and trace element and major oxides concentrations were measured by ICP-MS at the LEGS laboratory, Geological Sciences, University of Colorado Boulder.

3.7 Biosilicates Silicic hardparts of biota were isolated from bulk sediment using standard procedures outlined in full in Wallis (2001), including heavy liquid flotation, oxidation of organic matter, and acid removal of carbonates. Primary silicic fossils recovered were phytoliths, diatoms, and sponge spicules.

3.8 Surveys All surveying was accomplished with a Wild Total Station, which was set up at several sites along the crater rim. Each profile was tied to a temporary benchmark we established. Absolute elevations are based on topographic maps and are probably ±4 m, whereas the differences in elevation are accurate to within ±10 cm.

4. Sampling program

Samples were collected from strategic sites within and outside the crater. Locations of key sites are shown in Figures 6, 7, and 8.

4.1 Within crater samples A leveled east-west cross section through the crater is given in Figure 7; an inset with greater vertical exaggeration shows the topography adjacent to the central pan and the four main augered holes that were used to reconstruct the evolution of the sediment fill.

4.1.1 WCC99-04 (-19.17166; 127.79561) Assisted in 1999 by indigenous helpers from Billiluna, we completed a 9.8 m augered hole through the center of the crater pan (Fig. 6). Samples equivalent to about 3 cm of sediment depth were collected from 109 auger drives, at an average depth spacing of 9 ± 5 cm. Splits from most levels were analyzed for volume and mass MS, %C and $\delta^{13}C$ of bulk sediment, and hygroscopic moisture. At six roughly evenly spaced levels through the hole, samples were separated for, major and trace element and major oxide analyses, and a subset of sediment from nine levels were analyzed for mineralogy by X-ray diffraction.

4.1.2 01WCC-02 (-19.17166; 127.79561) In 2001 we used a Jacro 105 hydraulic coring unit to recover intact sediment between 5.8 and 6.3 m depth from the central pan. No other samples were recovered from the central pan.

4.1.3 01WCC-03 (-19.17169; 127.79699) This augered hole, situated 150 m east and at the same elevation as 01WCC-02, is at the eastern margin of the central pan (Fig. 7). The goal was to test whether the gypsum-rich upper unit logged in 99WCC-04 was of constant thickness. 01WCC-03 penetrated the base of the gypsum layer at 351 cm, 130 cm higher than in the central crater core. Below 351 cm the sediment consisted of gray clayey fine sand, with oogonia, the calcified fruiting bodies of charaphyte algae, present in some levels, consistent with an aquatic setting. Oogonia were isolated for ^{14}C dating from 363 cm depth (Table 1). Red sand grains were encountered at 508 cm, first seen in 99WCC-04 at 540 cm, with stringers of red sandy clay recovered at 520 cm, similar in character to sediment in 99WCC-04 at 580-600 cm. The differences in depth to buried stratigraphic units confirm that the crater has not always had a flat central pan. The hole was terminated at a depth of 598 cm.

4.1.4 01WCC-P1 (-19.17165; 127.79771) This auger hole, 2.4 m above the central pan, was to determine the thickness of the alluvial sand fan between the central pan and the east crater wall, and the nature and depth of the underlying sediment. The first 300 cm were featureless red sand, followed by 20 cm of browner sand, with gypsum encountered at 320 cm, 80 cm below the gypsum surface of the central pan. Gypsum continued until the hole was terminated at 345 cm.

4.1.5 01WCC-P2 (-19.17283; 127.79330) This auger hole, 3.3 m above the central pan, was placed at the line of trees visible in Figure 6, to determine the thickness of the sand fan, and the nature and depth of underlying sediment. The first 150 cm were fine red sand, then yellower sand and increasing clay content with depth. Gypsum-cemented sand was encountered at 429 cm, 1 m below the surface of the modern pan, and the hole was abandoned.

4.1.6 Lacustrine carbonates (-19.17456; 127.7962 and -19.1747; 127.7963) Patchy, thin lacustrine carbonates (tufa) were found encrusting rocks where the sandy crater fan intersects the crater wall over a horizontal distance of ~15 m and an elevation range of ~1 m (Fig. 6). Lacustrine carbonates are biologically mediated carbonate encrustations on rock surfaces near the surface of perennial water bodies. The encrustations are <1 cm thick, irregular, and with high porosity, but relatively common. Two samples were scraped from

rocks near the lower limit of algal carbonates, 3.5 m above the central pan (L1), and two others were collected from rocks at their upper limit, 4.5 m above the central pan (L2).

4.2 Dune Samples outside the crater Dune sediment deposited as a result of crater wall disruption of sand transport patterns were sampled both north and east of the crater rim.

4.2.1 North longitudinal dune (-19.1661; 127.7894) The northern arm of the horseshoe dune is larger, with a better-defined crest than the southern arm. A site on the crest of the northern arm, ~440 m from the crater rim (Fig. 8) was selected for an augered hole. A surveyed cross section (Fig. 9) reveals an asymmetry in dune form, suggesting that the upper 4 m are likely the result of active reworking of sand from the flanks toward the crest, and might reflect a slight net northerly component in the drift direction.

Two holes, one meter apart, were augered through dune sand and into a mixed ferricrete/sand layer between 9 and 10 m depth. The initial hole (01WCC-13) reached 10 m depth, from which 105 samples, each integrating ~3 cm of sediment were collected with an average depth spacing of 9.5 ± 1.3 cm. From the bulk samples, splits from most levels were separated for bulk MS, %clay and MS of the clay fraction, as well as bulk, sand, silt, and clay %C and $\delta^{13}C$ of that carbon. Samples were separated for grain size analyses at six levels. Samples for OSL were taken in companion hole 01WCC-14 centered on 100, 198, 388, 610, and 833 cm depth; the three deepest levels were dated by OSL.

4.2.2 Sand ramp at the eastern edge of the crater rim (01WCC-04 through -12) The prevailing easterly winds have built a sand ramp against the eastern rim of the crater wall. At the lowest point in the crater rim the sand ramp reaches rim height, and provides ingress of saltated sand into the crater where it forms an apron reaching the central pan. Nine holes were excavated along two transects eastward from the eastern crater rim, some by augering, others with the Jacro 105 hydraulic rig (Fig. 10).

5. Results: Central pan sediment fill (WCC99-04 and 01WCC-02)

We identify five sedimentary units in WCC99-04 (Fig. 11), constrained by geochronology, and physical and chemical characteristics.

5.1 OSL dates Two samples from Unit 4 recovered in the 01WCC-02 core were dated by OSL. Unit 4 was 90 cm thick in WCC99-04. The Jacro core recovered 52 cm of Unit 4, but we lack constraints on where in the 90 cm section this is from. We estimate it was from the middle of the unit, because it contains sediment only of Unit 4 character. After removing 8 cm from each end of the 52 cm core barrel, 15 cm of sediment was removed from each end for OSL analysis, leaving 8 cm of sediment between the two samples. The OSL sediment was homogenized, resulting in OSL samples that are 23 cm apart.

Because water content attenuates the dose rate, assumptions about water content history are required to derive an accurate sample age. Assuming the *in situ* water content is the long-term average, the ages are 30.3 ± 1.2 ka for the upper sample, and 31.2 ± 1.2 ka for the deeper sample. Although the sediment is currently water saturated, we argue below that the unit was deposited when the water table was below the depositional level. Given that the preliminary OSL ages indicate the unit is of Last Glacial Maximum (LGM) age, and the lowest oogonia date above the unit indicates perennial water by 13.4 ka, we recalculate the

OSL age assuming negligible (5%) water content until 14 ka, and then a saturated (*in situ*) water content after that date. The resulting ages are 28.1 ± 1.2 ka and 28.6 ± 1.2 ka respectively (Table 2). We accept the ages with variable water content as most likely to be correct, and transfer them to 6.3 and 6.6 m depth, about the middle of Unit 4 in WCC99-04 (Fig. 11).

5.2 Radiocarbon dates Four samples of oogonia were dated by AMS ^{14}C. There is no trace of calcite in the bedrock, suggesting that a hardwater effect for carbonate shells precipitated from groundwater is unlikely. Two extracts of oogonia from 75 cm in WCC99-04 were dated to evaluate reproducibility; the results (both ~5.6 ka) are nearly indistinguishable at $\pm 1\sigma$ (Table 1). Oogonia from 367 cm depth in WCC99-04 returned a date of ~11.2 ka. Oogonia extracted from sediment at 363 cm in 01WCC-03, at the eastern edge of the central pan (Fig. 7) are from gray clayey sand 17 cm below the lowest gypsum at an equivalent stratigraphic level of 500 cm in WCC99-04. The oogonia returned an age of 13.4 ka, which is used to constrain the chronology of WCC99-04.

5.3 Magnetic susceptibility (MS) Down-core variations in MS (Fig. 11) are unchanging over tens of cm but show abrupt changes between units, supporting the stratigraphic integrity of the augered samples. The high MS through Unit 4 (6.0 - 6.9 m) represents a depositional setting not repeated during any other interval preserved in the hole. Four brief, elevated MS levels in the upper four meters align with darker sediment interpreted to be paleosols during the coring. All sediment below 6.9 m depth has a near-uniform MS that is significantly higher than in Units 2 and 3, consistent with a different source and/or depositional environment.

5.4 Sedimentary organic matter Sedimentary $\delta^{13}C$ values and %C were determined on 89 bulk sediment samples between 69 and 980 cm depth (Fig. 12). Carbon concentrations were <1% in all levels, but sediment in Unit 1 had higher concentrations and greater variability than in Units 2-5, with muddy gypsum having the highest %C. The $\delta^{13}C$ values in Unit 1, the Holocene, are for the most part between -18.0 and -20.2‰, and consistently the most positive through the upper 2 m. In contrast, $\delta^{13}C$ in Units 2-5 lack a clear central tendency. Sedimentary $\delta^{13}C$ values range over 9‰, but without systematic differences between units or trends within or between units. They suggest highly variable conditions for vegetation within the crater over a wide range of timescales.

5.5 Hygroscopic moisture Hygroscopic moisture was measured on 31 sediment samples spaced on average 30 cm apart through 99WCC-04 (Fig. 12). These measurements correlate with Units on the core log defined by other physical properties, with Unit 1 (gypsum) having consistently high hygroscopic moisture, whereas Units 2, 3, and 4 have far less, and Unit 1 consistently even less (Fig. 12).

5.6 Sediment properties The insoluble fraction of the sample collected 0.8 m below the surface of a central pan sinkhole in 1979 consisted of 93% gypsum, 2% lo-Mg calcite, 3%

mud and 1% silica sand. From the small fraction of soluble salts, 84% was gypsum with smaller amounts of mirabolite and aphthitalite, a potassium sulfate mineral. Crater wall rock collected at the same time and analyzed by XRD is primarily α–quartz, with minor clay components, dominated by dickite, a polymorph of kaolinite, but little potassium.

Bulk sediment from nine depths in hole 99WCC-04 was analyzed for major and trace elements and major oxides by ICP-MS. While there are significant differences through the nine samples, the most relevant are the major oxides Fe_2O_3, MgO and Al_2O_3, which support the correlation between MS and iron concentrations, and the dominance of gypsum in Unit 1, with aluminosilicates more abundant in the deeper levels (Fig. 13).

Nine samples through WCC99-04 were analyzed for mineralogical composition by XRD (Table 3). Samples above 4 m depth are dominated by gypsum, but the darker, high-MS levels (Fig. 11) have significant levels of clay minerals, with illite/smectite ~3 times more abundant that kaolinite. Below 4.8 m depth (Units 2-5) the sediment is dominated by quartz, except for Unit 4, which has slightly more clay minerals than quartz; clay minerals consist of nearly equal proportions of illite/smectite and kaolinite.

5.7 Biosilicates

Biosilicates were isolated from units 1, 2, 4, and 5 (Fig. 11). Phytoliths were present in all samples at concentrations similar to other sediment in the region (Wallis, 2000), with good preservation except in Unit 4, where the phytolith surfaces exhibit circular dissolution pits, evidence of extreme chemical weathering, in contrast to phytoliths in units 2 and 5 that show no evidence of chemical weathering. Diatoms were present in Unit 5, and fragments of freshwater sponge spicules were present in units 2 and 5, indicative of primary sedimentation in perennial water.

6. The central crater sediment fill (WCC99-04 and 01WCC-02; Figs. 7 and 11)

The series of augered holes through the sand fans within the crater (holes 03, P1, P2; Fig. 7), demonstrate that there was no flat central pan at the end of the LGM. Rather, the LGM crater floor was more U-shaped (Fig. 7), and the floor has been leveled subsequently by gypsum precipitate through the Holocene, initially as an expanding pan, but eventually contracting steadily in circumference through the late Holocene, as the sand fans slowly aggraded by alluvial transport of pre-impact dune sand incorporated in the crater walls.

Based on physical characteristics of the sediment fill we identify four sedimentary units in WCC99-04. Unit 1, the upper 4.8 meters of the central pan is mostly gypsum, precipitated from groundwater, with up to 3 to 5% quartz sand and mud. Muddy (darker) layers with matching increases in magnetic susceptibility, indicating higher proportions of non-gypsum sediment, which represent decreases gypsum accumulation rates and/or increased influx of clastic sediment and soil development. Sediment from 480 to 240 cm depth is massive gypsum, separated by ~0.4 m of muddy gypsum ~11 ka, suggesting a halt in what had been a rising water table in the crater. More common dark bands in the upper 2.4 m suggests a decrease in the water table rise, especially after ~6 ka. The oogonia date of 5.6 ka at 75 cm depth, gives a sedimentation accumulation rate (SAR) of 13 cm ka^{-1} over the past 5.6 ka, whereas the average SAR between 13 and 5.7 ka was 55 cm ka^{-1}. Oogonia from 367

cm dated ~ 11.2 ka, indicate that the gypsum SAR was most rapid between 13 and 11.2 ka (63 cm ka^{-1}).

Clastic sediment between 480 and 540 cm (Unit 2) is gray, very fine clayey sand. The lack of red-stained quartz grains suggests water washing, and the identification of oogonia and fragmented sponge spicules confirm deposition in perennial water. Oogonia from the correlative sediment in 01WCC-03 date to 13.4 ka. Unit 2 sediment is underlain by 60 cm of redder, more clay-rich sand with stringers of darker red sandy clay (Unit 3) in the lower levels. Unit 3 terminates with an abrupt transition at ~600 cm to a more consolidated, dark red, sandy clay with traces of gypsum, 90 cm thick (Unit 4). We interpret Unit 4 to represent aeolian dust and sand delivered to a dry crater floor, as there is no evidence of water reworking of the sediment. Phytoliths from Unit 4 have dissolution pits indicative of extensive chemical weathering, whereas phytoliths from units 1 and 5 are fresh, without evidence of chemical weathering. Deposition of Unit 4 on a dry crater floor requires the water table to have been continuously more than 7 m below the modern pan surface throughout Unit 4 deposition and very likely overlying Unit 3 deposition.

The dark-red color of Unit 4 is linked to iron oxide coatings on quartz grains and/or clay-sized sediment mixed with iron and aluminum oxides (mostly hematite, goethite, kaolinite, and gibbsite). The high MS through Unit 4 is likely linked to the presence of maghemite and/or magnetite, which contribute to the peak. Maghemite/magnetite deposited directly on quartz grains before transport to the crater is preserved during aeolian transport by minor indentions in the grains, with smaller grains more efficiently preserving the clay coatings (Walker, 1967). Antiferromagnetic hematite and goethite do not have strong magnetic susceptibility. The two OSL dates described in section 5.2 were based on quartz grains 90-125 μm from the correlative unit in 01WCC-02, and are transferred to the middle of Unit 4 in 99WCC-04 (Fig. 11), confirming an early MIS 2 age for Unit 4.

We consider the entire sediment fill from 690 to 480 cm (Units 4, 3, and 2) to have been deposited during MIS 2 with the water table continuously deeper than 7 m below the modern pan surface during deposition of Units 4 and 3. Primary sediment properties are preserved in Unit 4, whereas overlying Unit 3 has been post-depositionally water modified. We hypothesize that the water table rose slowly late in MIS 2, with modest wave action partially working primary aeolian sediment similar to Unit 4 between 600 and 545 cm, an interpretation supported by the occurrence of stringers of intact Unit 4 sediment in Unit 3. These features suggest a fluctuating water table close to the crater surface at ~14 ka. The relatively low MS of Unit 3 may be a result of clays removed from sand grains by wave action, and translocated downward into Unit 4. Unit 2 represents LGM aeolian sediment modified syndepositionally by a water body. The presence of oogonia at these depths (13.4 ka) confirms at least shallow perennial water.

Pre-LGM Unit 5 sediment is separated from Unit 4 by an abrupt contact. We interpret Unit 5, which contains rare oogonia, trace levels of carbonate, and occasional gypsum to be aeolian sediment delivered to the crater when the floor was deep enough, and groundwater high enough, to maintain a permanent lake in the crater floor. A perennial water body is confirmed by oogonia, frustules of three different diatom taxa, and fragmented sponge spicules found in Unit 5 sediment.

7. Lacustrine carbonates document a high water level prior to 40 ka

The four lacustrine carbonate samples were dated by radiocarbon, giving calibrated ages that range from 25 ka to >40 ka (Table 1). Because of their high porosity, the samples have a high surface area to mass ratio, which makes them vulnerable to diffusion of younger carbon into the calcite crystals, a process that results in anomalously young ages. Similar concerns over the reliability of tufa dates beyond ~20 ka are reported by Preece et al. (1986), who report lacustrine carbonates with dates between 31 and 12 ka thought initially to record tufa formation during the LGM, that were later shown to be >33 ka, and almost certainly from the Last Interglaciation. More recently, Vazquez and Lidzbarski (2012) used $^{238}U/^{230}Th$ SIMS dating to demonstrate systematic age underestimations by ^{14}C dates on lacustrine carbonates, which they argue are compromised by recrystallization and open-system incorporation of younger carbon, especially for samples with actual ages close to or beyond the practical upper limit of ^{14}C dating.

Anticipating potential diffusion of younger carbon into the samples, each sample was leached with the stoichiometric addition of cold 2N HCl to remove ~90% of the mass before submission to the dating laboratory. However, the range of ages, and the conflict between a high water table at those ages and the evidence from the crater fill requiring much lower water levels, suggest that the highly porous nature of the carbonate and the efficient diffusion of younger carbon has compromised all four samples. We consider all four dates to be minimum ages, and that the lacustrine carbonates are beyond the range of ^{14}C dating.

7. The horseshoe dune sediment record (01WCC-13 and 01WCC-14)

From the longitudinal dune north of the crater (Fig. 8) augered hole 01WCC-13 recovered 10 m of sand, terminating on ferricrete. Companion hole 01WCC-14 was augered 1 m from 01WCC-13 to recover sediment for OSL dating. OSL ages from the three dated levels increase regularly with depth: 21.9 ± 1.6 ka at 388 ± 5 cm, 67.6 ± 3.4 ka at 610 ± 5 cm, and 107 ± 6 ka at 833 ± 5 cm (Table 2). Assuming no abrupt changes in sedimentation rate, a chronology for the aeolian sediment was derived by fitting a smoothed spline through the OSL dates (Fig. 14) using CLAM (Blaauw, 2010). The extrapolated age for the ferricrete contact at 996 cm is 138 ± 7 ka, which we consider to represent a maximum age for dune deposition and hence, for crater formation. However, as detailed below, we interpret the lowest meter to represent instantaneous deposition from the impact event, and the start of "continuous" aeolian sand deposition to occur at ~9 m depth, the base of Unit 3, ~120 ka, which is the most likely date of crater formation.

Bulk sediment MS was measured in 105 replicate sub-samples at ~10 cm intervals through 01WCC-13 (Fig. 15A). The rapid increase in MS below 9 m reflects the presence of ferricrete fragments. The MS of clay and %clay (sediment <3.9 μ□) was measured in 59 levels, spaced ~20 cm apart, but more closely in the lowest meter (Fig. 15B,C). Detailed particle size analyses from 6 levels (Table 3) indicate the upper 5 m are ~98% sand, with proportions of silt and clay increasing at almost equal rates below 6 m depth, resulting in the sand fraction reduced to ~80% in the lowest meter. Based on measured physical characteristics we identify four stratigraphic units in 01WCC-13 (Fig. 15).

The lowermost one meter, Unit 4, consists of clay-rich sand with common ferricrete fragments too large to be transported by wind, and strong changes in bulk sediment MS. We

consider Unit 4 to represent ejecta from the bolide impact, unrelated to the overlying longitudinal dune, and only preserved because the horseshoe dune began to form immediately after impact shielding the ejected sand and finer grains from aeolian deflation. Bedrock ejecta traveled primarily in an easterly direction.

Unit 3 is bracketed by ages of ~120 and ~85 ka, corresponding with MIS 5. It has consistent physical characteristics (Fig. 15) that contrast with younger units, and with the ejecta debris beneath. Unit 3 represents the onset of horseshoe dune formation resulting from the impactor landing near the center of a longitudinal dune, and the crater wall deflecting the prevailing easterly winds. The average SAR is similar through Unit 3 and overlying Unit 2 deposition at ~5 cm ka^{-1}.

Unit 2 is bracketed by ages of ~85 and ~14 ka, corresponding to MIS 4, 3, and 2, with physical characteristics transitional between underlying Unit 3 and overlying Unit 1. Clay MS exhibits a steady increase from values similar to those in underlying Unit 3 at the base, to values consistent with Unit 1 values by the top of Unit 2.

Unit 1, the upper 3.1 m, essentially the narrow, active longitudinal dune, has a higher average SAR of 22 cm ka^{-1}. Clays from Unit 1 have a high, and near constant MS confirming a very different source for the finest grain sizes than in MIS 5. Bulk sediment MS, on the other hand, declines through Unit 1.

Sedimentary $\delta^{13}C$ was measured in sand, silt and clay separates, from 48 levels through Units 1, 2, and 3 spaced ~20 cm apart, and at ~10 cm intervals through Unit 4. Unit 4 had insufficient carbon in most sand and silt separates for reliable $\delta^{13}C$ measurements, but the high concentrations of clay provided sufficient carbon, with the $\delta^{13}C$ values in clay from eleven levels through Unit 4 averaging -19.2 ± 1.4‰, more negative than clay separates from any of the overlying units. Unit 3 has only slightly less negative $\delta^{13}C$ in the clay fractions (-18.6‰), and the most negative $\delta^{13}C$ in the other three size fractions (Fig. 16). The mean $\delta^{13}C$ in all grain-size separates from Unit 2 is intermediate between Unit 3 and Unit 1, without any trend with depth through the dune. Sedimentary $\delta^{13}C$ in the uppermost two meters is the most positive in all grain-sizes across all four units.

8. Discussion

Physical, chemical and isotopic data archived in sediment recovered in 10 m deep holes both inside and outside the crater provide evidence of substantial environmental change in and around the crater since its formation, related primarily to changes in effective moisture, presumably dominated by systematic changes in the strength of the Australian Summer Monsoon.

8.1 The Crater's sedimentary fill Changes in sediment character in the augered hole from the center of the crater document changes in sediment sources interacting with a variable water table and steadily rising central pan surface. The uppermost ten meters of sediment in the central pan spans the past ~60 ka. The available sedimentological, geochemical, and geochronologic data, combined with geomorphic contexts suggest that the crater fill has the potential to provide a continuous record of monsoon strength through most of the Late Quaternary.

The dominant sediment sources to the crater are the aeolian transport of sand and dust from the east, chemical precipitates concentrated from dissolved salts in groundwater, and pre-impact red dune sand that was incorporated in the crater walls and subsequently eroded by wind and rain to create alluvial fans that are impinging on the central crater pan. Only minor additions are from weathered crater wall rock. Given that crater wall rock contains only kaolinite polymorphs, whereas clays in the upper 4 m of crater fill contain three times more illite/smectite than kaolinite, and in roughly equal concentrations at deeper levels, we conclude that most of the clay in the crater floor must have been delivered by aeolian transport of clay minerals from the east, a conclusion supported by the analysis of clay minerals in dust samples from NW Australia that are dominated by kaolinite and illite (Gingele et al., 2001).

Whereas the sediment properties in WCC99-04 are controlled by processes operating outside the crater, the organic matter in WCC99-04 is primarily local, and highly dependent on the evolving relation between the crater fill surface, the within-crater water table, and its salinity. Organic matter contributions to crater sediment include terrestrial plants such as Eucalyptus or Acacia, salt-tolerant plants, and aquatic microbial sources.

Sedimentary $\delta^{13}C$ values in the gypseous mud of Unit 1 are the only interval with a tightly clustered central tendency, averaging -18.6 ± 0.4‰. Within the nearly pure gypsum portion of Unit 1, $\delta^{13}C$ values are more variable, ranging from -17.3 to -21.3‰, without a well-constrained central value. Below the gypsum $\delta^{13}C$ values are even more variable, ranging over 11‰, and without any obvious differences between Units 2, 3, 4 and 5. The lack of between unit differences is unexpected, but the high variability in $\delta^{13}C$ values suggests continuously variable conditions for vegetation within the crater over a wide range of timescales.

8.2 Groundwater fluctuations over the past 60 ka The crater floor acts as a window into the regional groundwater. The regional groundwater surface slopes to the south, mimicking the land surface that slopes southward at 1 m km^{-1}. The water table within the crater is set by the regional water table, reduced within the crater by evaporative drawdown processes. The regional water integrates annual rainfall over a large region upbasin of the crater on decadal to centennial timescales. Reconstructing the magnitude of past declines in the regional water table from the sediment fill is challenging because the water level within the crater can be reduced by local evaporative processes that may vary over time, and the surface of the infilling sediment is rising on millennial timescales. Estimating past regional water table rises is less ambiguous, with evidence of high water levels within the crater requiring a regional water table at least at that elevation, and possibly higher.

Within these constraints we use evidence from the crater to derive a tentative reconstruction of water table changes over the past ~60 ka (Fig. 17). We infer that the current central pan surface represents the mean late Holocene water table, which we set as a base level at 327.5 m asl[3]. Unit 5, the lowermost three meters in WCC99-04, represents aeolian sediment deposited in, and reworked by a perennial water body, with a water level above 320

[3] Absolute elevations are ±4 m, whereas differences in elevation are, for the most part, accurate to ±0.1 m.

m asl, and likely much higher. The abrupt Unit 5/4 contact suggests that the water table fell rapidly below 320 m asl before 35 ka, after which 1.4 m of iron-rich desert dust and sand (Units 4 and 3) was deposited on a perennially dry crater floor with regional groundwater continuously ≥7 m below the Late Holocene level.

Increased rainfall beginning ~14 ka raised the water table, which intercepted the crater floor at 322 m asl before 13 ka. We suspect that the water-table rise was slow, allowing modest wave action to partially modify sediment that was initially similar to Unit 4, despite little fetch to develop wave action, producing Unit 3. By the Unit 3/2 boundary, groundwater had risen sufficiently to create a perennial lake in the crater, and although desert sand and dust similar to that found in Units 4 and 3 continued to be deposited in the crater, the water table was high enough for wave action to efficiently rework the sediment as it was deposited, producing Unit 2, with oogonia dated to 13.4 ka. An early onset of the summer monsoon ~14 ka is consistent with other evidence in the region suggesting strong monsoon rains began about that time (van der Kaars and DeDeckker, 2002; van der Kaars et al., 2006; Wyrwoll and Miller, 2001).

By ~12 ka aeolian deposition within the crater had effectively ceased. The lack of clastic sediment input to the crater, coupled with a rising table and sufficient wind speed to transport sand and dust (Fig. 3), suggests that renewed rainfall had allowed vegetation to recolonize and stabilize longitudinal dune systems east of the crater. The increased rainfall caused the water table to rise more rapidly than before, resulting in gypsum -precipitation (Unit 1) without any mixing of the gypsum with underlying Unit 2. The lack of mixing indicates that by 12 ka the water level was high enough that wave action could not modify sediment at 322.7 m asl. Two meters of massive gypsum were interrupted once by increased fine siliclastic sediment deposited in shallow water, with oogonia dated to 11.2 ka, which we interpret to reflect a stable water table at 324 m asl. The water table continued to rise after 11 ka, and another meter of massive gypsum was precipitated, followed by a final two meters of gypseous mud. The surface of the central pan stabilized at about the current level shortly after 6 ka. Whether the early Holocene (11 to 6 ka) water table was significantly above the current pan floor is unknown. However, lacustrine carbonate incrustations on rock surfaces 331 to 332 m asl with ^{14}C ages from 25 to >40 ka document a water table 3.4 to 4.5 m above the average Late Holocene level. Although the ages remain indeterminate, the high water event certainly predates the LGM, and we speculate that the lacustrine carbonates are of MIS 5 age, equivalent to the highest Late Quaternary water level for KT-LE (Magee et al., 2004; Cohen et al., 2011).

8.3 A dusty LGM The Unit 5/4 boundary defines the onset of strong aridity. Unit 5 was deposited in perennial water and has less clay than any of the LGM Units (4, 3, 2). The abrupt Unit 5/4 contact requires a rapid drop in the local water table at about the MIS 3/2 boundary. Collectively, Units 4, 3, and 2 document 2 m of aeolian sediment delivered to the crater in ~15 ka, between 30 and 15 ka. The sediment in these units is dominated by dust-sized (silt and clay) clastic grains, consistent with regional aridity, but not necessarily higher wind speeds. Throughout Units 4 and 3 iron-rich clay, silt, and fine sand were transported to the crater by easterly winds when the crater floor was U-shaped, without a flat central pan. We interpret Unit 2 to have the same primary aeolian source, but the sediment was

extensively reworked by a shallow water body in the crater as the regional water table rose late in the MIS 2.

Although the Wolfe Creek Crater evidence for peak aridity during MIS 2 is similar to other regions of the Australia Arid Zone (Hesse et al., 2004; Fitzsimmons et al., 2013), evidence for substantial LGM dust transport in northern Australia is less apparent. Bowler (1976) postulated two major dust pathways, an eastward trajectory for southern Australian dust and a westward trajectory for northern Australian dust. An MIS 2 dust peak in marine cores east of southern Australia (Hesse et al., 2004; Fitzsimmons et al., 2013) supports the southern dust flux, but the few marine cores sampled west of northern Australia do not show a similar MIS 2 dust maximum (Hesse and McTainsh, 2003; Fitzsimmons et al., 2013). A possible resolution to this enigma is that the easterly trade winds weakened during the LGM, but cold and drought reduced or eliminated dune vegetation, destabilizing longitudinal dunes, and the weaker winds were limited to transporting primarily the finer grain sizes into the crater, with little dust reaching far out into Indian Ocean to the west.

8.4 Horseshoe dune sedimentary $\delta^{13}C$ constrains effective moisture since 120 ka. Sedimentary $\delta^{13}C$ in 01WCC-13 is set by the vegetation growing on and around the horseshoe dune and some distance to the east. Sedimentary $\delta^{13}C$ values are converted to $\%C_4$ plant contribution to the measured isotopic value based on the $\delta^{13}C$ values measured in living plants in and around the crater (Fig. 16), with a C_3 end member having a $\delta^{13}C$ value of 26.5 ± 0.6‰, and a C_4 end member $\delta^{13}C$ value of -12.0 ± 1.6‰ (Wooller *et al.,* 2005).

The average $\delta^{13}C$ value of all four grain-size separates in Unit 3 is -21.2 ± 0.9‰, characteristic of a C_3-C_4 mixed woodland and grassland, with 60 to 80% C_3 trees and shrubs, indicative of more effective moisture than at present. The $\delta^{13}C$ values in all three grain-size separates from Unit 2 are intermediate between Units 3 and 1, without any trend with depth through the dune. The mean $\delta^{13}C$ value for all grain sizes, -19.9 ± 1.2‰, is indicative of an average vegetation assemblage that has fewer C_3 trees and shrubs than in underlying Unit 3.

Sedimentary $\delta^{13}C$ in the uppermost two meters is the most positive in all grain-sizes across all four units (Fig. 16), averaging -17.3 ± 1.8‰, characteristic of a dominantly C_4 grass environment, similar to the present landscape. The lowermost meter of Unit 1 has sedimentary $\delta^{13}C$ similar to Unit 2 in all grain-size categories.

The overall trend in sedimentary $\delta^{13}C$ is consistent with a first-order decline in effective moisture through the past 120 ka. Plants respond strongly to changes in effective moisture, the balance between precipitation and evaporation. Because MIS 5 sediment has sedimentary $\delta^{13}C$ indicative of a dominant contribution from C_3 trees and shrubs, we suggest this is the most favorable interval for plant life in terms of effective moisture. This conclusion is consistent with algal carbonates indicative of high water levels in the crater some time before 40 ka. We postulate that during MIS 5 summer monsoon rains were the strongest of the past 120 ka, producing an elevated water table, and supporting a mixed woodland and grassland, which was extant when the crater was formed.

8.5 Eastern sand ramp record suggests impact trajectory from the west Nine holes, ranging from 90 to 180 m distant from the eastern crater rim, were hand-augered or drilled

hydraulically to determine the thickness of the sand ramp built up against the crater wall by westerly aeolian sand transport. In all nine holes impenetrable fractured bedrock mixed with ferricrete was encountered between 3 and 5 m depth, generally shallowest closest to the crater wall (Fig. 10). This finding contrasts with the western rim, where the crater wall is at a steep angle, descending almost 30 m to intact ferricrete terrain over a horizontal distance of <100 m, whereas the highest point on the eastern rim descends less than 18 m over a horizontal distance of 250 m (Fig. 10). Where the sand ramp reaches the crater rim at its lowest point, the sand is only 4 m thick, and rests on jumbled bedrock fragments. This pattern is consistent with an impactor hitting the landscape from the west to northwest expelling most of the bedrock debris eastward, where it accumulated on the eastern flank of the crater wall. Our dataset contrasts with observations by Shoemaker et al. (2005), on the crater's elliptical form, surface ejecta pattern, and dominance of meteoritic material on the southwest side of the crater that led them to conclude an oblique trajectory of the impactor from the northeast.

8.6 A revised estimate for the age of Wolfe Creek Crater Shoemaker et al. (1990) based their estimate for the meteorite impact that created the crater on radionuclide ratios in a meteorite fragment found some distance from the crater that indicated the impact occurred ~300 ka. We have taken a different approach on constraining the impact age, using the basal age of the horseshoe dune outside the crater as the onset of systematic deflection of aeolian sand transport by the crater wall, and using the age of the sediment fill within the crater as a minimum age estimate.

The oldest secure dates from the crater's sediment fill are two OSL dates of ~28 ka from Unit 4. Assuming all of Units 2, 3, and 4 were deposited during MIS 2, and the base of Unit 4 sediment is ~35 ka, the MIS 2 sedimentation rate is ~10 cm ka^{-1}. Applying that rate to the 2.9 m of sediment in Unit 5 produces a basal age of ~60 ka. Given that there is an unknown thickness of sediment below Unit 5, we consider 60 ka to be a minimum age for crater formation.

The horseshoe dune places more secure constraints on crater formation. Assuming relatively constant sedimentation, the extrapolated basal age of 01WCC-13 is 138 ± 7 ka (Fig. 14). However, Unit 1 contains common variably sized ferricrete pebbles too large to have been transported by wind, and strongly variable physical properties (Fig. 15). Consequently, we interpret Unit 1 to be a preserved remnant of impact ejecta. Most of the impact debris is located east of the crater, with little debris north of 01WCC-13. But, because the bolide impacted close to the crest of a longitudinal dune (Fig. 4), there would have been a wide scatter of dune sand and ferricrete, forming a ferricrete-rich sand sheet across the landscape. Most of the sand deposited in the inter-dune swales, would have been efficiently remobilized by wind. Easterly winds would also have relatively quickly begun to deposit the basal layers of the horseshoe dune, preserving the impact debris beneath it. With this interpretation, the basal age of Unit 2 at 900 cm depth, 120 ± 5 ka may be considered a close estimate for the date of crater formation. Given that there is some uncertainty on the actual contact between impact debris and aeolian dune sand, we propose that 120 ± 10 ka is a more secure age for the formation of Wolfe Creek Crater.

These ages are younger than the most widely cited age for crater formation of 300 ka (Shoemaker et al. 1990). That age is dependent on the meteorite fragment found on the ground surface some distance from the crater being an actual remnant of the meteorite that formed the crater. Given uncertainties linking the fragment to crater formation, we consider our new data a more reliable estimate of the crater-forming event. We argue that crater formation certainly occurred after 138 ± 7 ka, and most likely 120 ±10 ka, but certainly before ~60 ka. These estimates suggest that the sediment fill within the crater has been continuously accumulating for the past 120 ka, and has the potential to provide an exceptional record of monsoon activity through the Late Quaternary.

8.7 Rate of dune extension Based on our revised estimates for the age of meteorite impact, we can calculate the rate of dune extension in this region, a parameter that is logistically difficult to determine. There are few other dune extension studies against which to compare our estimate. A partly vegetated longitudinal dune in the Simpson Desert showed no apparent extension between 2006 and 2012 in the 'Millennium Drought' affecting Australia (Craddock et al., 2015). Cohen et al. (2010) showed that a source-bordering dune adjacent to a Cooper Creek palaeochannel in the Strzelecki Desert had not extended progressively but grown by vertical accretion, similar to the conclusion of studies in the northern Simpson Desert (Hollands et al., 2006; Bristow et al., 2007). These studies have led to the contention that longitudinal dunes, generally, grow by vertical accretion and 'wind-rifting' rather than by extension (Hollands et al., 2006). At a different temporal and spatial scale, Pell et al. (1999; 2000; 2001) found that there was no evidence of transport of sand between the large sand seas in Australia, in contrast to speculations made in the Sahara (Wilson, 1971).

Assuming that the impact disturbed a pre-existing longitudinal sand dune, and that primary western advance of the horseshoe dune is by extension, we can calculate a rate of dune extension from our data. We estimate the length of dune extension as the distance between the upwind edge of the crater and Wolfe Creek (~3 km), in which the dune now terminates. This is a minimum possible transport distance because the creek prevents further downwind aeolian transport. The rate of dune extension is derived by dividing the extension distance by the age of the impact. Because the crater created the obstacle resulting in deflection of the dune, the impact age (120 ka) is the maximum age of the horseshoe dune. We also make the simplifying assumption that the time span over which the dune extended is 120 ka, even though it is plausible that the horseshoe dune reached Wolfe Creek earlier when there was sparse vegetation cover and greater sand transport. The derived dune extension rate, ~35 m ka^{-1}, is therefore a minimum rate because the distance is a minimum estimate but the time span estimate is a maximum estimate. The vertical accretion rate at the sample location is nearly constant at 5 cm ka^{-1} through MIS 5 - 2, and about 20 cm ka^{-1} for the narrow upper 3 m deposited during the Holocene.

The rate of dune extension derived here (~35 m ka^{-1}) is similar to that found by Telfer (2011) in the Kalahari for a vegetated longitudinal dune, similar to Australian dunes, which extended ~210 m across a pan between ~12 ka and 7 ka at a rate of 42 m ka^{-1}. Like Telfer (2011), we infer low rates of longitudinal dune extension in this presently marginal desert dunefield, but that there is also evidence of vertical accretion, at least episodically, possibly by reworking of sand previously eroded from the dunes themselves (Fujioka et al., 2009). On

longer timescales, an extension rate of ~35 km Ma^{-1} suggests dune extension during the Quaternary was likely to have been ~100 km, given that our estimate is conservative.

9. Conclusions

On Quaternary timescales changes in effective moisture across the northern Australian arid zone are a direct response to changes in the strength of the Australian Summer Monsoon. The findings in this study support previous arid-zone studies that conclude Late Quaternary climate was relatively wet during portions of MIS 5, with significantly less moisture subsequently. There is evidence for wet intervals during MIS 3, but not as wet or as persistent as during MIS 5, followed by persistent aridity after ~50 ka, with exceptionally cold, arid conditions during MIS 2, but only a weak intensification of monsoon rains during the Holocene. This leads to the "Holocene climate enigma". Although substantial evidence is available that the early Holocene experienced increased wetness relative to MIS 2, there is no evidence that monsoon rains approached those recorded ~50 ka, despite the primary variables for strong monsoon flow, high sea level, elevated sea surface temperatures, and strong land-sea pressure gradients, were more favorable in the Holocene than at any time during MIS 3.

We sought to address this enigma directly by evaluating the rainfall record recorded by climate proxies preserved in the sediment fill in the Wolfe Creek Crater, and in the deflected longitudinal dune outside the crater. We sampled the past 60 ka of sediment within the crater that allowed the development of a 60 ka water-table record. Relative wetness 60-35 ka was abruptly terminated ~35 ka, as reflected in a rapid water table drop within the crater to more than 7 m below the Late Holocene level, consistent with a very dry LGM. A rise in the water table beginning ~14 ka, is consistent with the early onset of monsoon rain ~14 ka recorded elsewhere in northern Australia. Lacustrine carbonates more than 40 ka old and 3.5 to 4.5 m above the late Holocene water level confirm a regional water table higher than any time during the Holocene, which we suggest occurred during MIS 5 (bracketing ages are >40 ka and <120 ka).

Sediment recovered in a 10 m hole through the horseshoe dune outside the crater revealed a basal meter of impact debris, overlain by 9 m of aeolian sediment, with the basal age of the aeolian sediment (120 ka) providing the first direct date on crater formation, considerably younger that a previous estimate (300 ka). The $\delta^{13}C$ values of sedimentary organic matter preserved in the aeolian sediment document a mixed C_3/C_4 woodland during MIS 5, a shift toward increasing dominance of C_4 plants through MIS 4, 3, and 2, and a nearly pure C_4 vegetated landscape in the Holocene, confirming a stronger summer monsoon during MIS 5 than at any time subsequently and the lack of persistent effective moisture comparable to MIS 3 during the Holocene.

Both the proxy climate data from within the crater, and from the dune outside the crater are consistent with a stronger summer monsoon throughout MIS 5, and even into MIS 4 and 3 than at any time during the Holocene. The explanation for a weakened summer monsoon response to imposed external forcing (sea level, sea surface temperature, and orbitally paced insolation changes that result in changing land-sea pressure gradients) remains obscure.

10. Acknowledgements

The Aboriginal elders in Billiluna are thanked for permission to conduct our research in and around Wolfe Creek Crater. Individuals from Billiluna assisted in transporting equipment into and out of the crater in 1999. The Department of Conservation and Land Management (CALM) is thanked for technical permits NE002182 and NE002617 authorizing the field activities in and around the crater, and fo9r guidance in delivering the hydraulic coring rig to the crater rim in 2001. We thank Sean Pack for assistance in the 1999 field season. The 2001 season included 15 scientists on site; the authors thank Linley Wallace, Stephen DeVogel, Monique Belanger, Elizabeth Miller, Andrew Wilkie, Gillian Atkin, and Dan Grossman for their contributions during fieldwork at the crater. Damien Kelleher is thanked for his expert efforts at getting the Jacro coring rig into the crater and extracting core from within and outside the crater. Norman Hill and Danielle Questiaux are thanked for their assistance with the OSL dating sample preparation and data analysis respectively. The 1999 field season was funded by the US National Science Foundation grant AGS-502632 to GHM and MLF, and the 2001 field season was funded jointly by the US National Science Foundation grant AGS-082254 to GHM and MLF, the Australian Research Council to JWM, and the Australian National University funded the coring rig and personnel to operate. We thank Monique Belanger, Wendy Roth, Denis Eberl, and Patrick De Deckker for analytical results of the augered sediment, and Jim Caldwell is thanked for chemical and mineralogical analyses of 1979 samples.

11. Literature Cited

Blaauw, M. (2010) Methods and code for “classical” age-modelling of radiocarbon sequences, *Quaternary Geochronology*, 5: 512–518. doi:10.1016/j.quageo.2010.01.002.

Bowler, J. M. (1976) Aridity in Australia: age, origin and expression on aeolian landforms and sediments., *Earth Science Review*, 12: 279–310.

Bowler, J.M., Duller, G.A.T., Perret, N., Prescott, J.R., Wyrwoll, K.-H. (1998) Hydrologic changes in monsoonal climates of the last glacial cycle: stratigraphy and luminescence dating of Lake Woods, N.T., Australia. *Palaeoclimates* 3: 179–207.

Bowler, J. M., K. H. Wyrwoll, and Y. Lu. (2001) Variations of the Northwest Australia Summer Monsoon over the Last 300,000 Years: The Paleohydrological Record of the Gregory (Mulan) Lakes System. *Quaternary International* 82–85: 63–80. https://doi.org/10.1016/S1040-6182(01)00009-X.

Bristow, C.S., Jones, B.G., Hollands, C., Coleman, M., Price, D.M. (2007) GPR surveys of vegetated linear dune stratigraphy in central Australia: Evidence for linear dune extension with vertical and lateral accretion, in: Baker, G.S., Jol, H.M. (Eds.), Stratigraphic Analyses Using GPR. Geological Society of America Special Paper 432: 19-33.

Cassidy, W. A. (1954) The Wolf Creek, Western Australia, meteorite crater. *Metoeritics*, 1: 197–199.

Chen, X.Y., Bowler, J.M. and Magee, J.W. (2007) Late Cenozoic stratigraphy and hydrologic history of Lake Amadeus, a central Australian playa, Australian Journal of Earth Sciences, 40: 1-14, 10.1080/08120099308728059

Chivas, A., DeDeckker, P., Nind, M., Thiriet, D., Watson, G. (1986) The Pleistocene palaeoenvironmental record of Lake Buchanan: An atypical Australian playa. P*alaeogeography, Palaeoclimatology, Palaeoecology* 54: 131-152

Cohen, T.J., Nanson, G.C., Larsen, J.R., Jones, B.G., Price, D.M., Coleman, M., Pietsch, T.J. (2010) Late Quaternary aeolian and fluvial interactions on the Cooper Creek fan and the

association between linear and source-bordering dunes, Strzelecki Desert, Australia. *Quaternary Science Reviews* 29: 455-471.

Cohen, T. J. *et al.* (2011) Continental aridification and the vanishing of Australia's megalakes, *Geology* 39: 167–170. doi: 10.1130/G31518.1.

Cohen, T. J. *et al.* (2012) Late Quaternary mega-lakes fed by the northern and southern river systems of central Australia: Varying moisture sources and increased continental aridity, *Palaeogeography, Palaeoclimatology, Palaeoecology* 356–357: 89–108. doi:10.1016/j.palaeo.2011.06.023.

Craddock, R.A., Tooth, S., Zimbelman, J.R., Wilson, S.A., Maxwell, T.A., Kling, C. (2015) Temporal observations of a linear sand dune in the Simpson Desert, central Australia: Testing models for dune formation on planetary surfaces. *J. Geophys. Res. Planets* 120: 1736–1750. doi:10.1002/2015JE004892. □

Eberl, D.D., 2003. User guide to RockJock: A program for determining quantitative mineralogy from X-ray diffraction data: U.S. Geological Survey Open File Report 03-78, 40 pp.

English, P., Spooner, N.A., Chappell, J., Questiaux, D.G. and Hill. N.G. (2001) Lake Lewis Basin, Central Australia: Environmental Evolution and OSL Chronology. *Quaternary International* 82: 81–101. https://doi.org/10.1016/S1040-6182(01)00032-5.

Fitzsimmons, K.E., Miller, G.H., Spooner, N.A., and Magee, J.W. (2012) Aridity in the monsoon zone as indicated by desert dune formation in the gregory lakes basin, northwestern Australia, *Australian Journal Earth Sciences*, 59: 469-478. doi: 10.1080/08120099.2012.686171.

Fitzsimmons, K. E. *et al.* (2013) Late Quaternary palaeoenvironmental change in the Australian drylands, *Quaternary Science Reviews*, 74: 78–96. doi:http://dx.doi.org/10.1016/j.quascirev.2012.09.007.

Fudali, R. F. (1979) Gravity investigation of Wolf Creek Crater, Western Australia, *Journal of Geology*, 87: 55–67.

Fujioka, T., Chappell, J., Fifield, L.K., Rhodes, E.J. (2009) Australian desert dune fields initiated with Pliocene-Pleistocene global climatic shift. *Geology* 37: 51-54 10.1130/g25042a.1.

Gingele, F.X., DeDeckker, P., and Hillenbrand, C.D. (2001) Clay mineral distribution in surface sediments between Indonesia and NW Australia - source and transport by ocean currents. *Marine Geology* 179:135–46. https://doi.org/10.1016/S0025-3227(01)00194-3.

Grieve, R. A.F. and Pilkington, M. (1996) The signature of terrestrial impacts. *Journal Australian Geology and Geophysics*, 16: 399–420.

Guppy, D. J. and Matheson, R. S. (1950) Wolf Creek meteorite crater, Western Australia, *Journal of Geology*, 58: 30–36.

Halse, S.A., Pearson, G.B., and Kay, W.R. (1998) Arid zone networks in time and space: waterbird use of Lake Gregory in North-Western Australia. *Int. Journal Ecology Environmental Sciences*, 24: 207–222.

Hawke, P. J., (2003) Geophysical investigation of the Wolfe Creek Meteorite Crater: Western Australia Geological Survey, Record 2003/10, 9pp.

Hesse, P.P. and McTainsh, G.H. (2003) Australian dust deposits: modern processes and the Quaternary record. Quat. Sci. Rev., 22: 2007-2035. doi:10.1016/S0277-3791(03)00164-1.

Hesse, P. P., Magee, J. W. and van der Kaars, S. (2004) Late Quaternary climates of the Australian arid zone: a review. *Quaternary International* 118-119: 87–102.

Hesse, P. (2011) Sticky dunes in a wet desert: Formation, stabilisation and modification of the Australian desert dunefields, *Geomorphology*, 134: 309–325. doi:10.1016/j.geomorph.2011.07.008.

Hollands, C.B., Nanson, G.C., Jones, B.G., Bristow, C.S., Price, D.M., Pietsch, T.J., (2006) Aeolian-fluvial interaction: evidence for Late Quaternary channel change and wind-rift linear dune formation in the northwestern Simpson Desert, Australia. *Quaternary Science Reviews* 25: 142-162.

Johnson, B.J., Miller, G.H., Fogel, M.L., Magee, J.W., Gagan, M.K., and Chivas, A.R. (1999) 65,000 Years of Vegetation Change in Central Australia and the Australian Summer Monsoon. *Science* 284: 1150-1152. https://doi.org/10.1126/science.284.5417.1150.

van der Kaars, S. and DeDeckker, P. (2002) A Late Quaternary pollen record from deep-sea core Fr10/95, GC17 offshore Cape Range Peninsula, northwestern Western Australia. *Review Palaeobotany Palynology*, 120: 17–39. doi: 10.1016/S0034-6667(02)00075-1.

van der Kaars, S., DeDeckker, P. and Gingele, F. X. (2006) A 100,000-year record of annual and seasonal rainfall and temperature for northwestern Australia based on a pollen record obtained offshore. *Journal Quaternary Science*, 21: 879–889. doi: 10.1002/jqs.1010.

La Paz, L. (1954) Meteoritic material from the Wolf Creek, Western Australia, Crater. *Meteoritics* 1:200-203. 10.1111/j.1945-5100.1954.tb01332.x

Macumber, P.G. (1992) Hydrological processes in the Tyrrell Basin, southeastern Australia. *Chemical Geology*, 96: 1-18. doi: 10.1016/0009-2541(92)90118-O.

Magee, J.W., Miller, G.H., Spooner, N.A. and Questiaux, D. (2004) A continuous 150,000 year palaeomonsoon record from Lake Eyre, Australia, shows linkages to N. Hemisphere forcring and unexpected failure of the Holocene Monsoon, *Geology* 32: 885–888.

Mchone, J. F. *et al.* (2002) Space shuttle observations of terrestrial impact structures using SIR-C and X-SAR radars, *Meteoritics Planetary Science*, 37: 407–420. doi:10.1111/j.1945-5100.2002.tb00824.x.

Miller, G. H., Fogel, M. L., Magee, J. W. and Gagan, M. K. (2016) Disentangling the impacts of climate and human colonization on the flora and fauna of the Australian arid zone over the past 100 ka using stable isotopes in avian eggshell. *Quaternary Science Reviews*, 151: 27-57. doi: 10.1016/j.quascirev.2016.08.009.

O'Neill, C. and Heine, C. (2005) Reconstructuring the Wolfe Creek meteorite impact: Deep structure of the crater and effects on target rock, *Australian Journal Earth Sciences*, 52: 699–709. doi: 10.1080/08120090500170450.

Pell, S.D., Chivas, A.R., Williams, I.S. (1999) Great Victoria Desert: development and sand provenance. *Australian Journal Earth Sciences* 46:289-299.

Pell, S.D., Chivas, A.R., Williams, I.S., (2000) The Simpson, Strzelecki and Tirari Deserts: development and sand provenance. *Sedimentary Geology* 130: 107-130.

Pell, S.D., Chivas, A.R., Williams, I.S., (2001) The Mallee Dunefield: development and sand provenance. *Journal Arid Environments* 48: 149-170.

Preece, R. C., Thorpe, P. M. and Robinson, J. E. (1986) Confirmation of an interglacial age for the Condat tufa (Dordogne, France) from biostratigraphic and isotopic data. *J. Quaternary Sci.*, 1: 57–65. doi:10.1002/jqs.3390010107

Prescott, J.R. and Hutton, J.T., (1994) Cosmic ray contributions to dose-rates for luminescence and ESR dating: large depths and long-term time variations. *Radiation Measurements* **23:** 497-500.

Reeves, F., and Chalmers, R.O., (1948) The Wolf Creek crater. *Australian Journal Sciences*, 11: 145–146.

Reimer, P. J. et al. (2013) INTCAL13 and MARINE13 radiocarbon age calibration curves 0-50,000 years cal BP, *Radiocarbon*, 55: 1865–1887.

Shoemaker, C.S., Nishizumi, K., Kohl, C.P., Arnold, J.R., Klein, J., Fink, D., Middleton, R., Kubic, P.W., and Sharma P. (1990) Ages of Australian meteorite carters - A preliminary report., *Meteroitic*, p. 409.

Shoemaker, E.M., Macdonald, F.A., and Shoemaker, C.S. (2005). Geology of five small Australian impact craters, Australian Journal Earth Sciences, 52: 529-544. doi:10.1080/08120090500180921

Spooner, N.A., Olley, J.M., Questiaux, D.G. & Chen, X.Y. (2001). Optical dating of an aeolian deposit on the Murrumbidgee floodplains. *Quaternary Science Reviews* 20: 835-840.

Telfer, M.W., 2011. Growth by extension, and reworking, of a south-western Kalahari linear dune. *Earth Surface Processes and Landforms* 36: 1125-1135.

van der Kaars, S. and DeDeckker, P. (2002) A Late Quaternary pollen record from deep-sea core Fr10/95, GC17 offshore Cape Range Peninsula, northwestern Western Australia. *Review Palaeobotany Palynology* 120:17–39. https://doi.org/10.1016/S0034-6667(02)00075-1.

van der Kaars, S., DeDeckker, P. and Gingele, F.X. (2006) A 100,000-year record of annual and seasonal rainfall and temperature for northwestern Australia based on a pollen record obtained offshore. *Journal Quaternary Science,* 21: 879–89. https://doi.org/10.1002/jqs.1010.

Vazquez, J.A. and Lidzbarski, M.I. (2012) High-resolution tephrochronology of the Wilson Creek Formation (Mono Lake, California) and Laschamp event using ^{238}U-^{230}Th SIMS dating of accessory mineral rims. *Earth Planetary Science Letters*, 357–358: 54-67. doi.10.1016/j.epsl.2012.09.013.

Wallis, L.A. 2001 *Phytoliths, Late Quaternary Environment and Archaeology in Tropical Semi-arid Northwest Australia*. Unpub. PhD thesis,Archaeology and Natural History, Research School Pacific Asian Studies, Australian National University, Canberra.

Walker, T.R. (1967) Formation of red beds in modern and ancient deserts GSA Bulletin 78: 353-368. https://doi.org/10.1130/0016-7606(1967)78[353:FORBIM]2.0.CO;2

Wilson, I.G. (1971) Desert sandflow basins and a model for the development of ergs. *Geographical Journal* 137: 180-199.

Wooller, M. J. *et al.* (2005) Stable isotope characteristics across narrow savanna/woodland ecotones in Wolfe Creek Meteorite Crater, Western Australia. *Oecologia*, 145: 100–112. doi:10.1007/s00442-005-0105-5.

Wyrwoll, K.-H. and Miller, G. H. (2001) Initiation of the Australian summer monsoon 14,000 years ago. *Quaternary International* 83-85: 119-128. doi:10.1016/S1040-6182(01)00034-9.

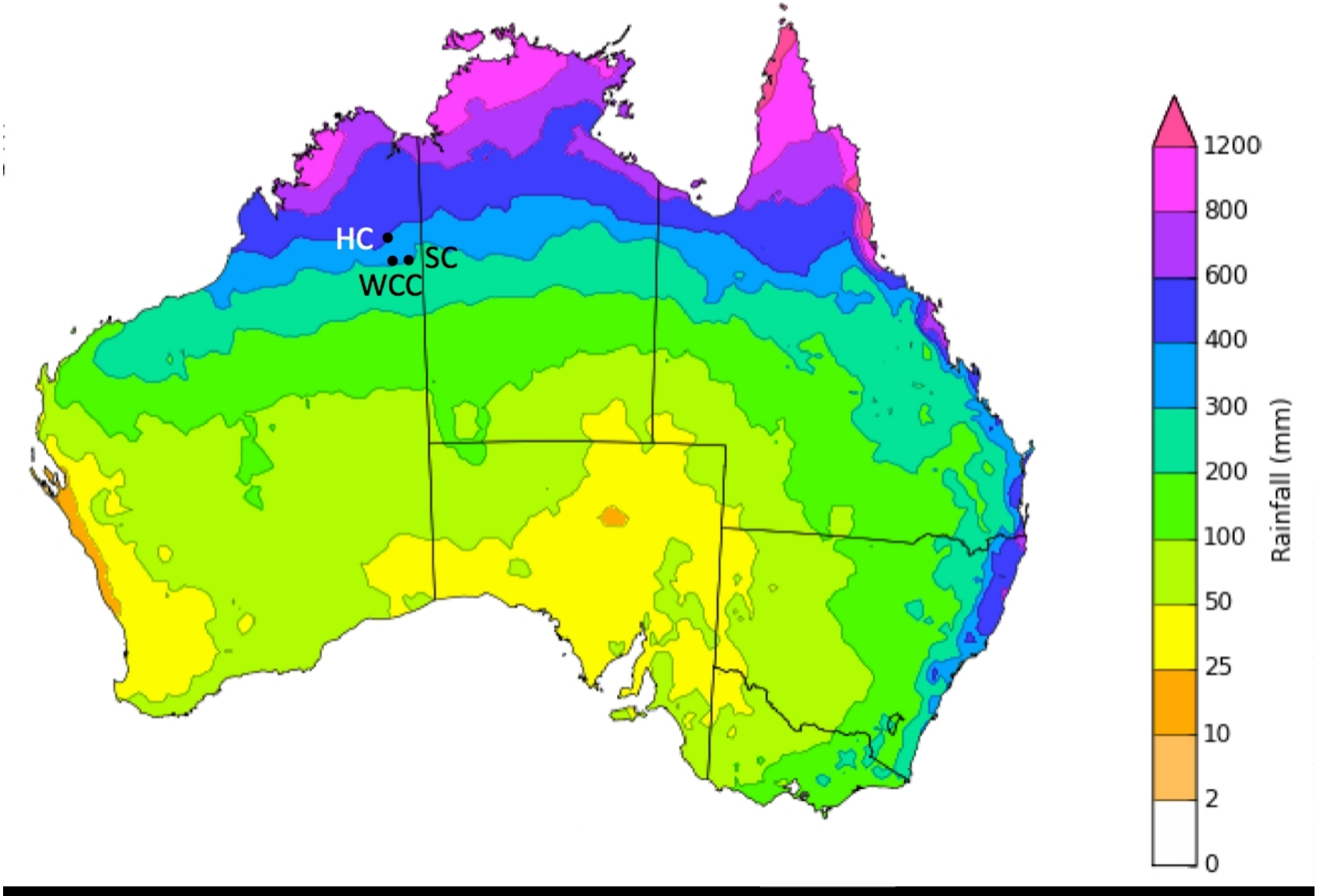

Fig. 1

Fig. 2

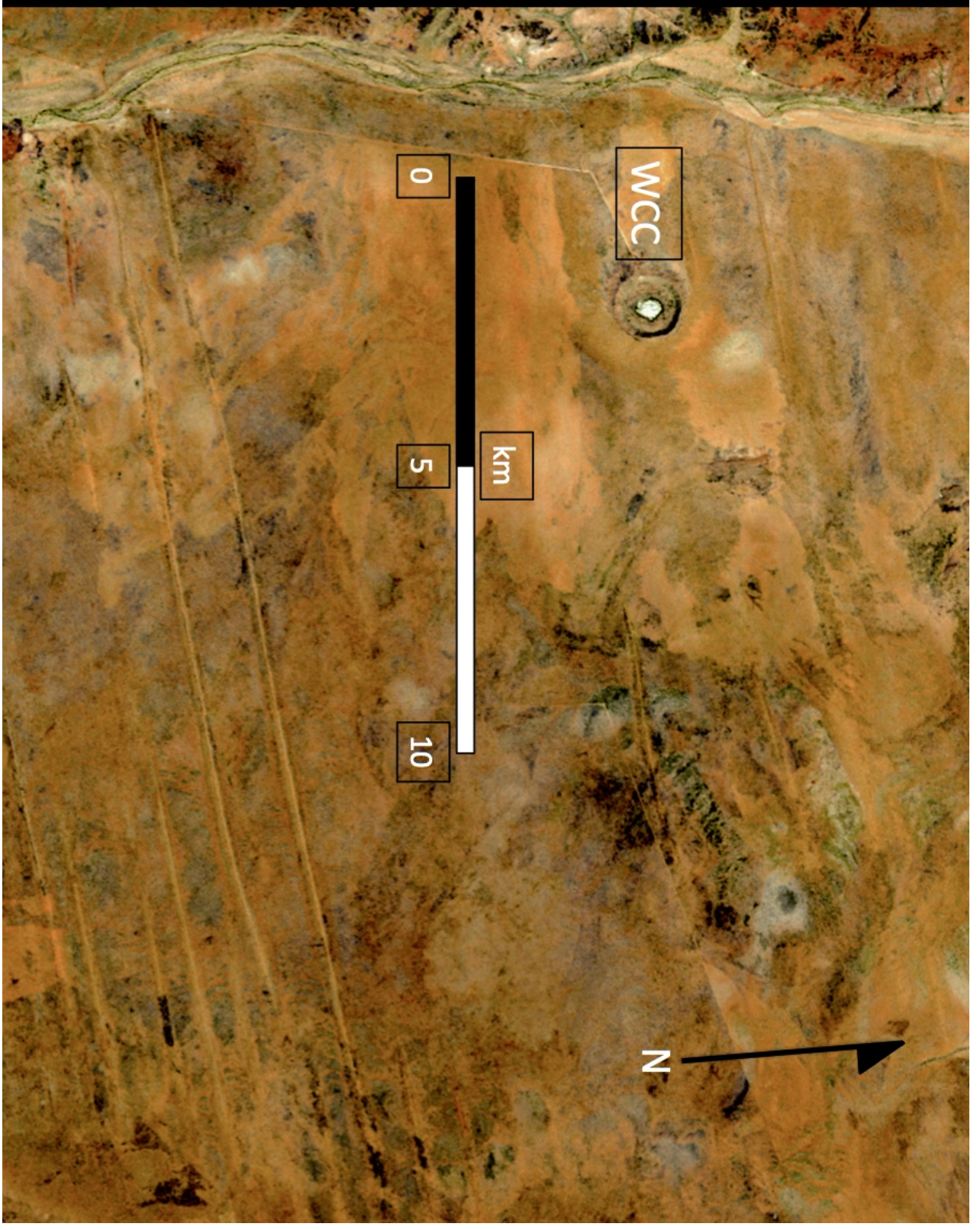

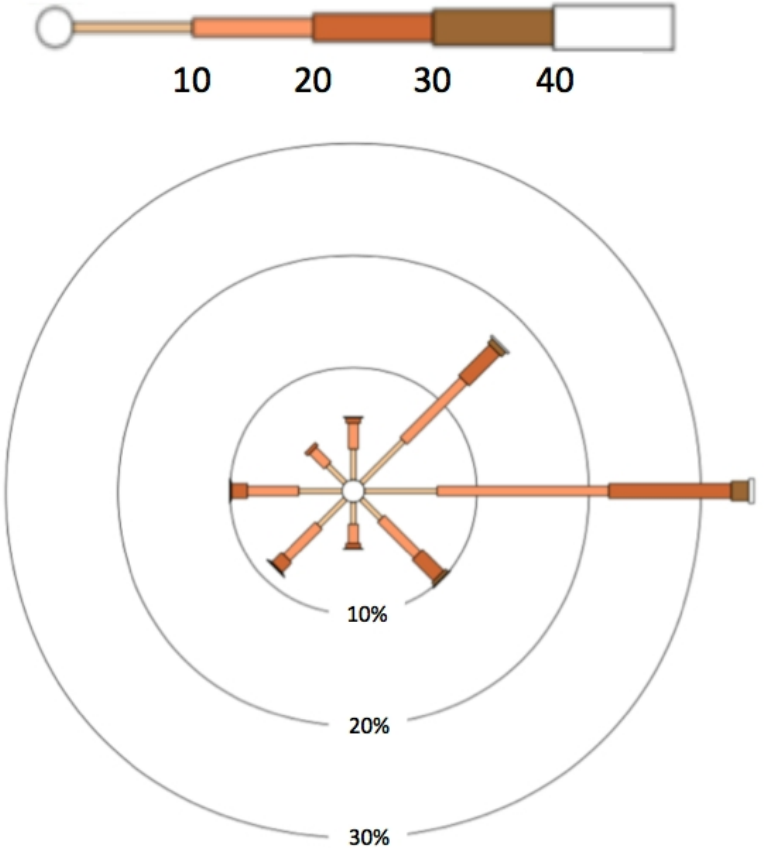

Fig. 3

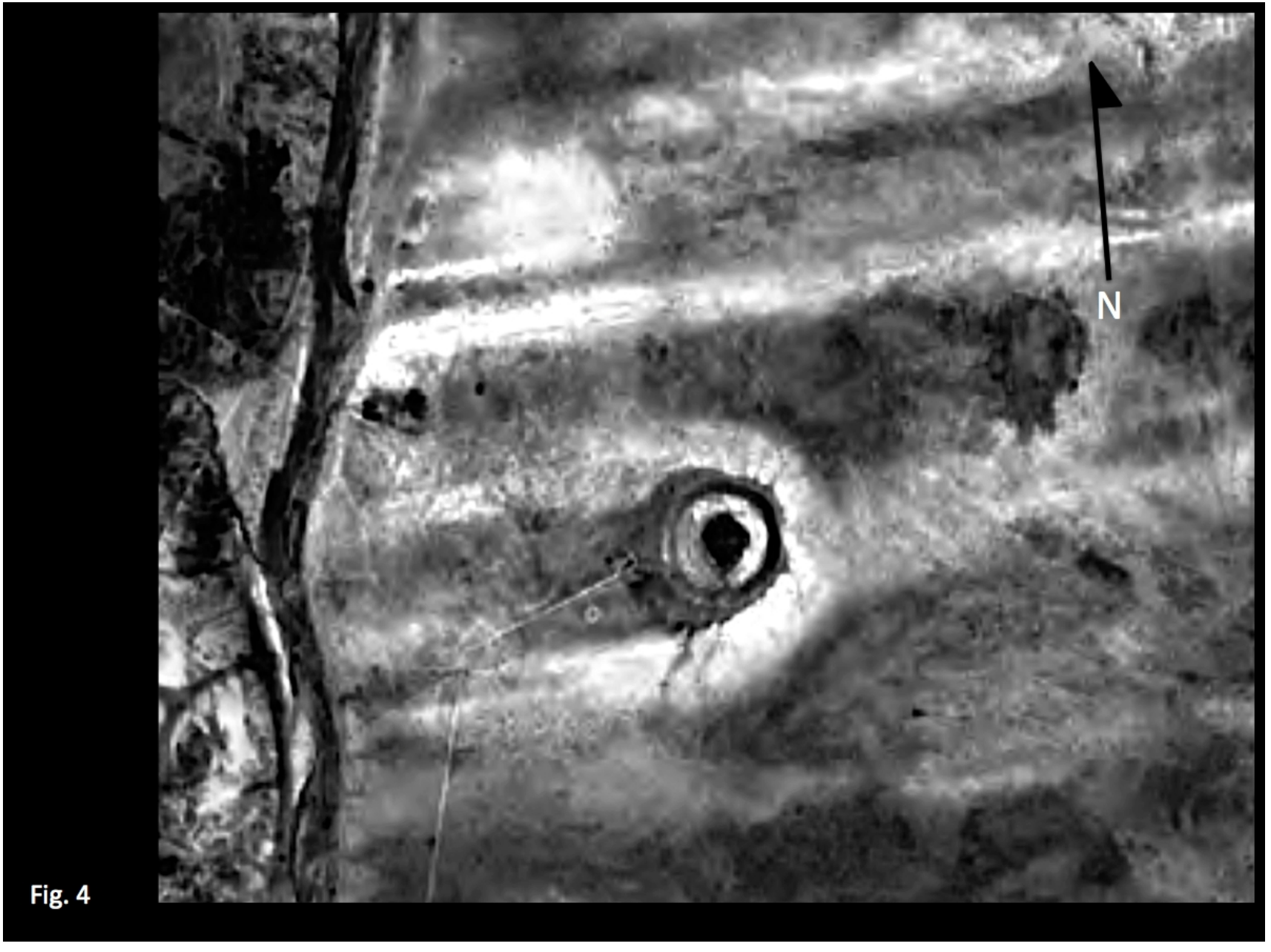

Fig. 4

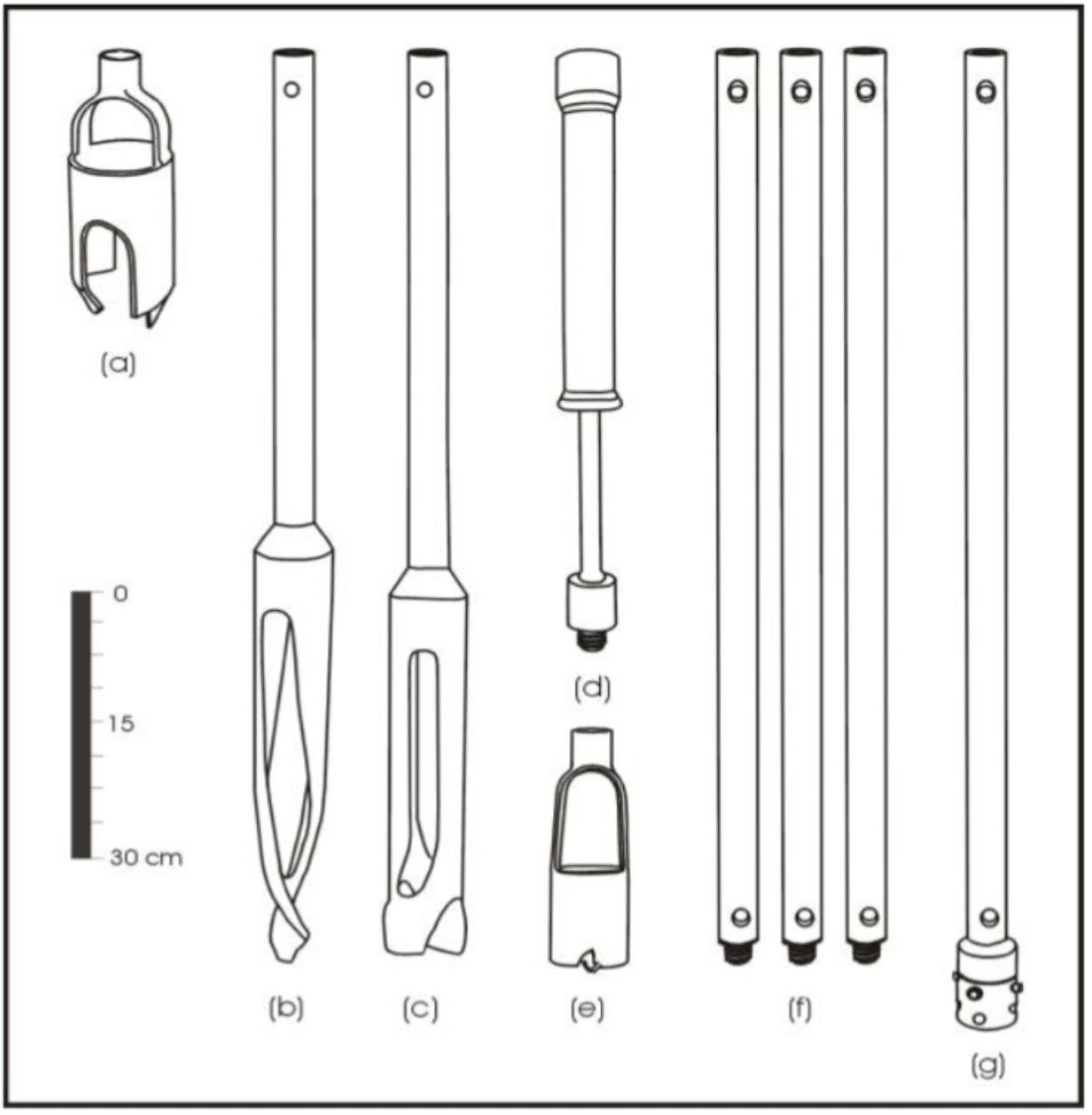

Fig. 5

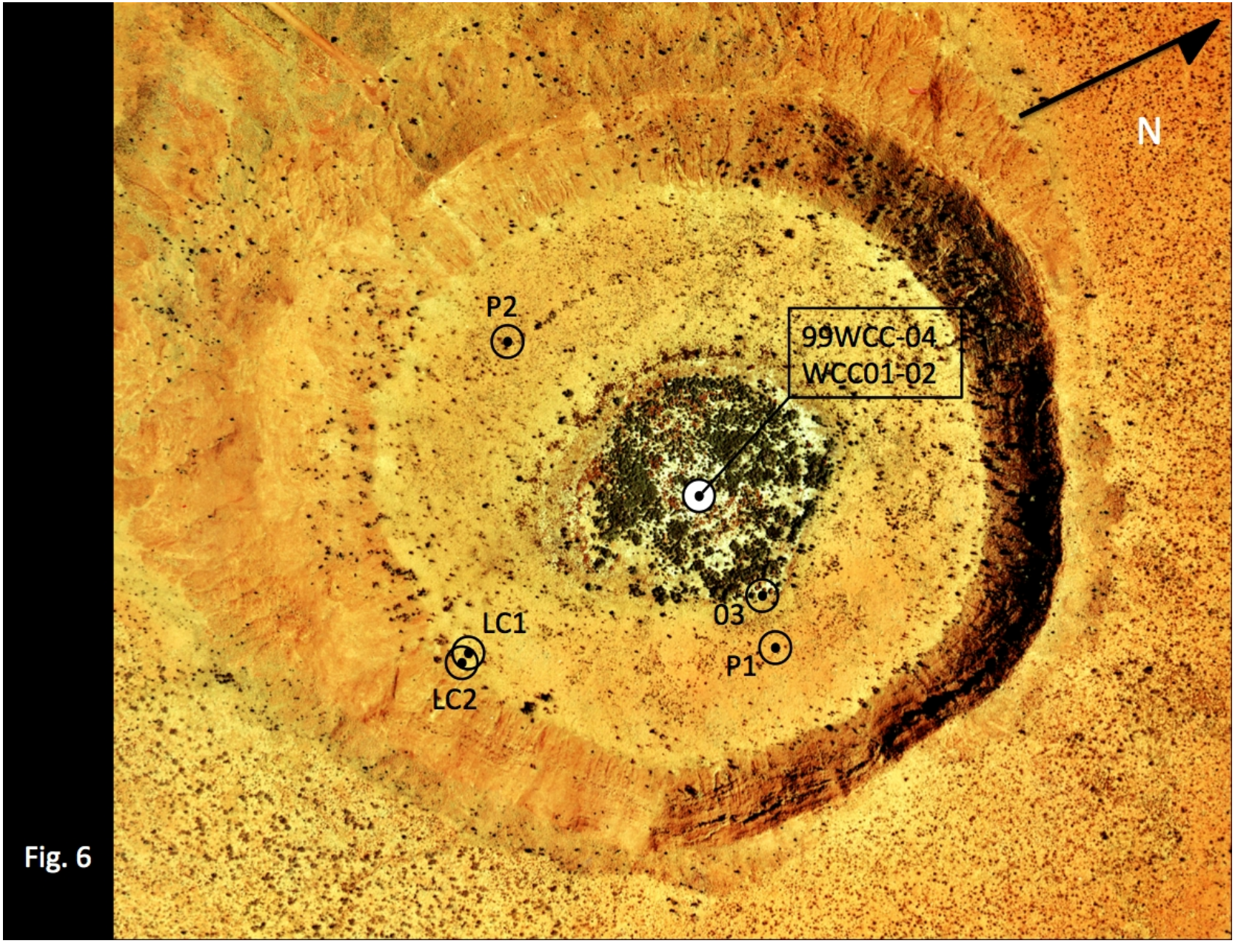

Fig. 6

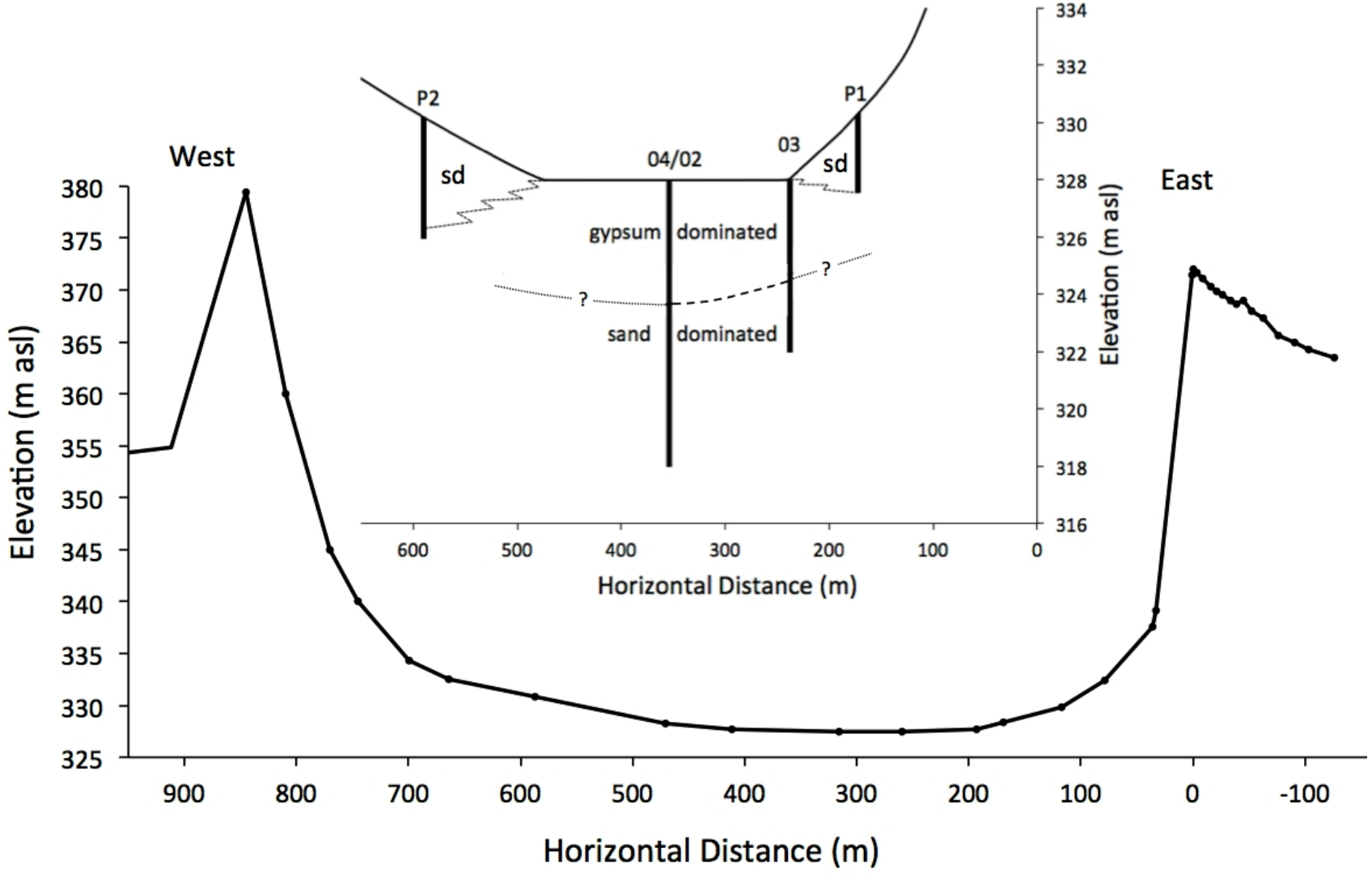
West
East
Elevation (m asl)
Horizontal Distance (m)
380
375
370
365
360
355
350
345
340
335
330
325
900
800
700
600
500
400
300
200
100
0
-100
P2
P1
03
04/02
sd
sd
gypsum dominated
sand dominated
?
?
334
332
330
328
326
324
322
320
318
316
600
500
400
300
200
100
0
Elevation (m asl)
Horizontal Distance (m)

Fig. 7

Fig. 8

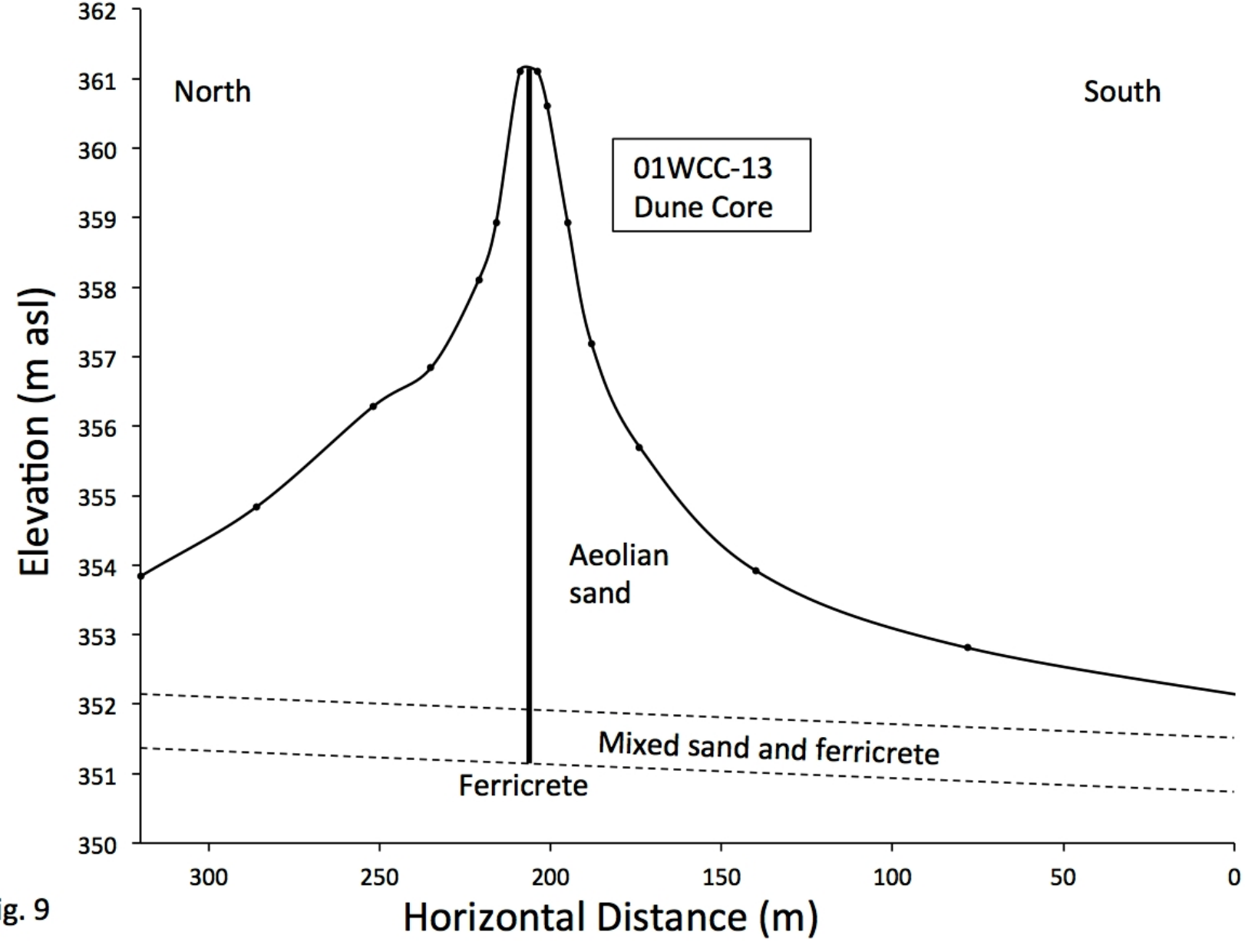
North
South
01WCC-13
Dune Core
Aeolian
sand
Mixed sand and ferricrete
Ferricrete
Elevation (m asl)
Horizontal Distance (m)
362
361
360
359
358
357
356
355
354
353
352
351
350
300
250
200
150
100
50
0

Fig. 9

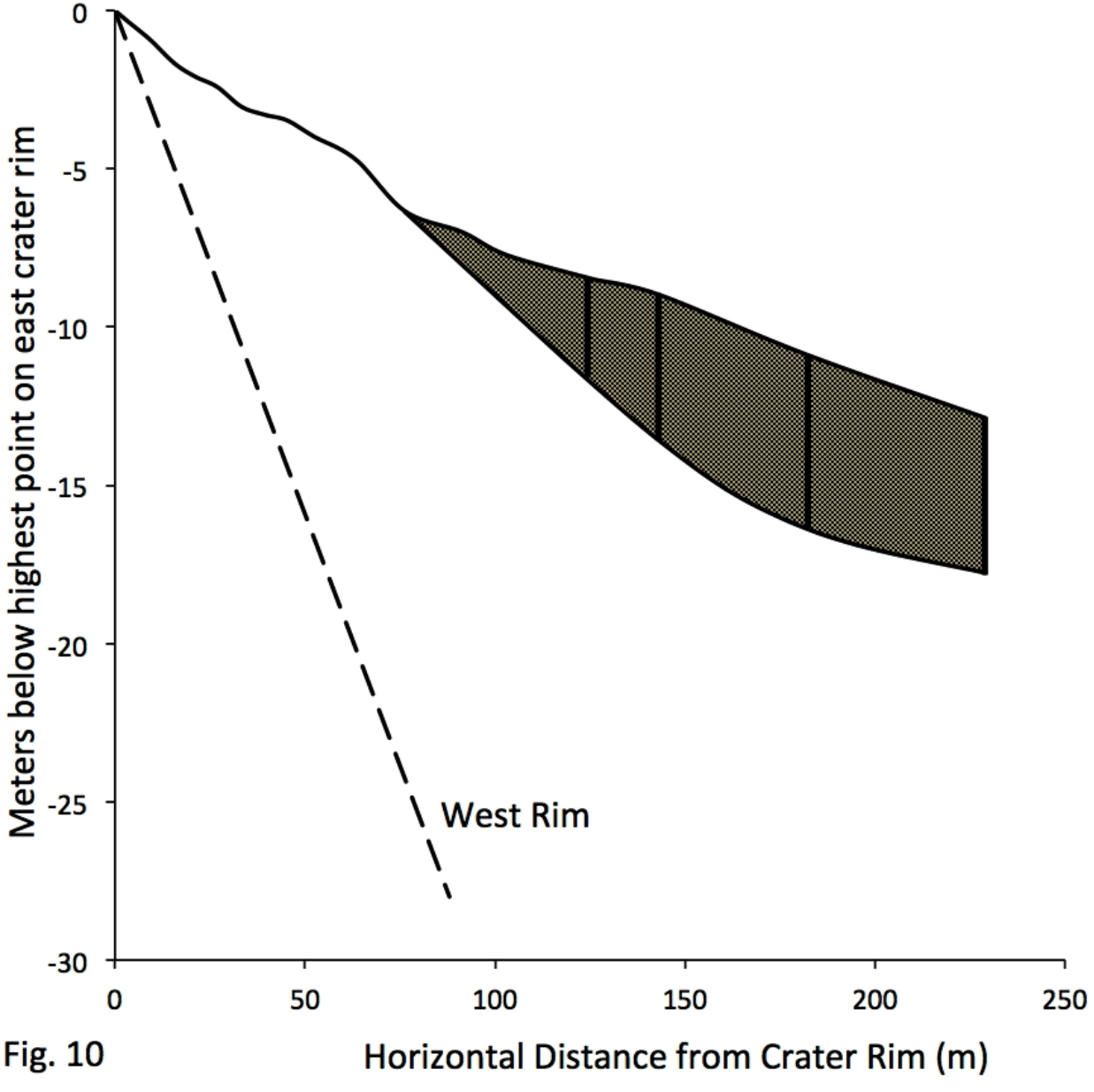
0
-5
-10
-15
-20
-25
-30
Meters below highest point on east crater rim
West Rim
0
50
100
150
200
250
Horizontal Distance from Crater Rim (m)

Fig. 10

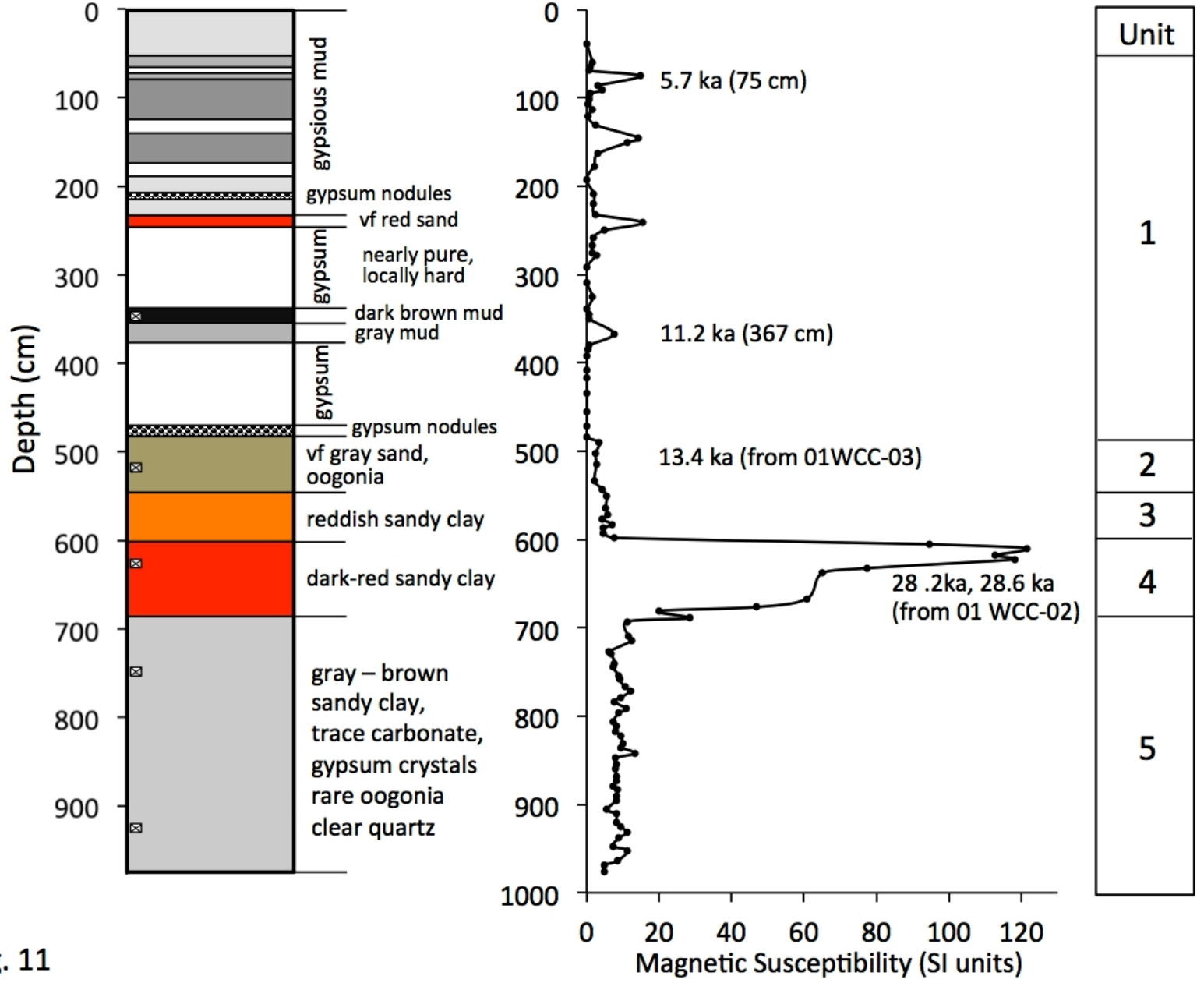
Depth (cm)
0
100
200
300
400
500
600
700
800
900
gypsious mud
gypsum nodules
vf red sand
gypsum
nearly pure,
locally hard
dark brown mud
gray mud
gypsum
gypsum nodules
vf gray sand,
oogonia
reddish sandy clay
dark-red sandy clay
gray – brown
sandy clay,
trace carbonate,
gypsum crystals
rare oogonia
clear quartz
0
100
200
300
400
500
600
700
800
900
1000
5.7 ka (75 cm)
11.2 ka (367 cm)
13.4 ka (from 01WCC-03)
28 .2ka, 28.6 ka
(from 01 WCC-02)
0
20
40
60
80
100
120
Magnetic Susceptibility (SI units)
Unit
1
2
3
4
5

Fig. 11

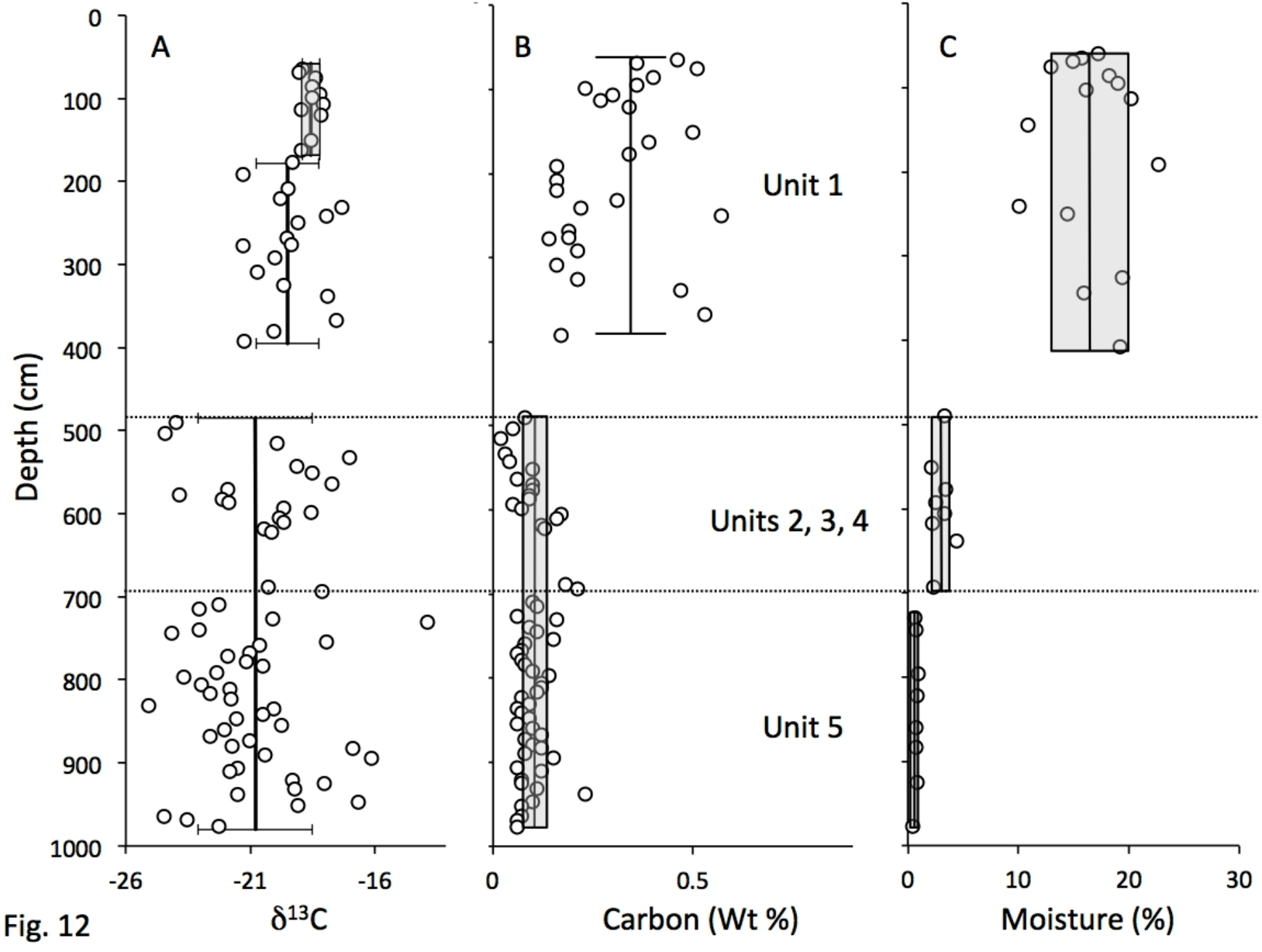
A
B
C
Depth (cm)
0
100
200
300
400
500
600
700
800
900
1000
Unit 1
Units 2, 3, 4
Unit 5
-26
-21
-16
δ13C
0
0.5
Carbon (Wt %)
0
10
20
30
Moisture (%)

Fig. 12

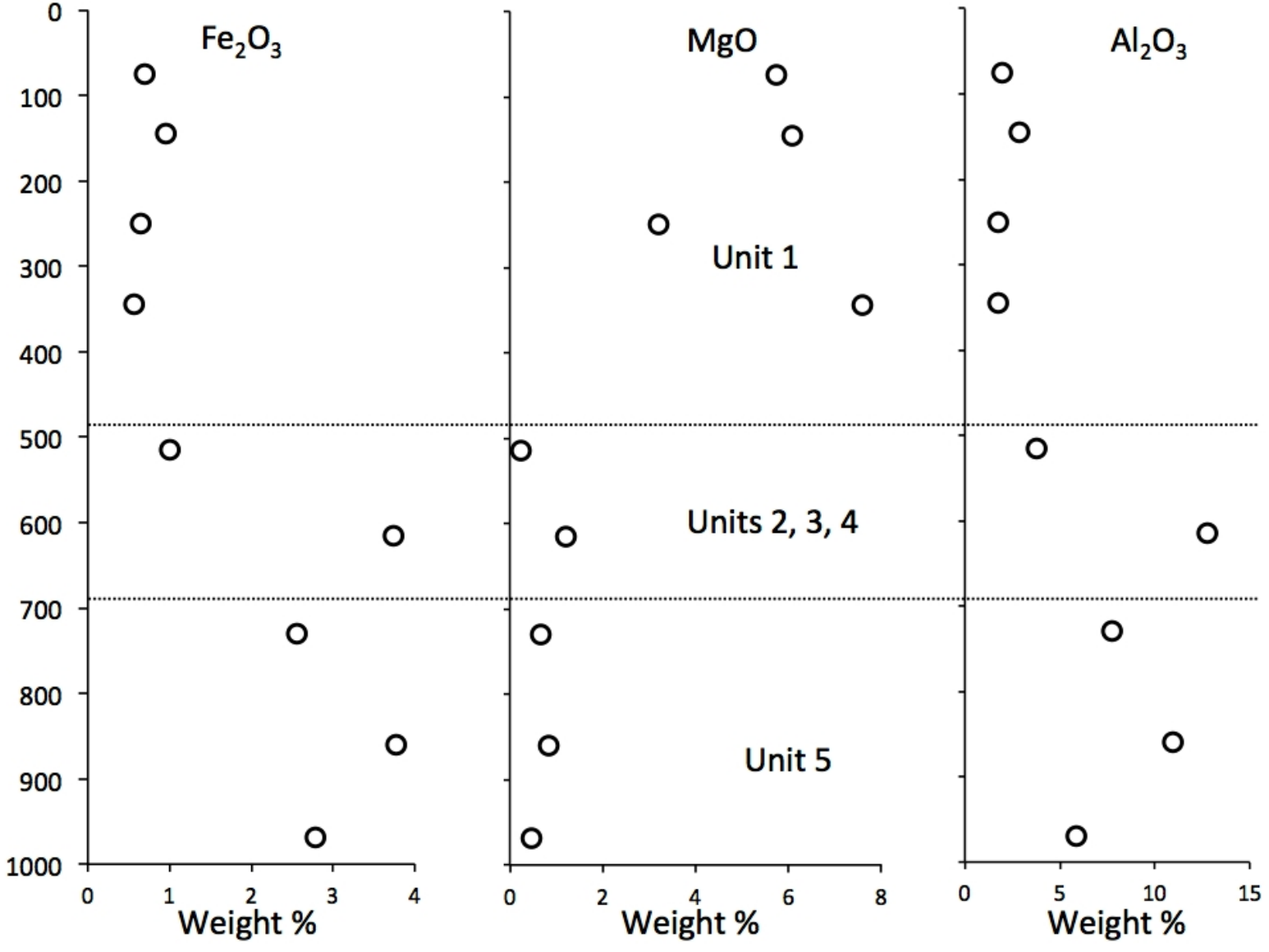
Fe_2O_3
MgO
Al_2O_3
Unit 1
Units 2, 3, 4
Unit 5
0
100
200
300
400
500
600
700
800
900
1000
0
1
2
3
4
0
2
4
6
8
0
5
10
15
Weight %
Weight %
Weight %

Fig. 13

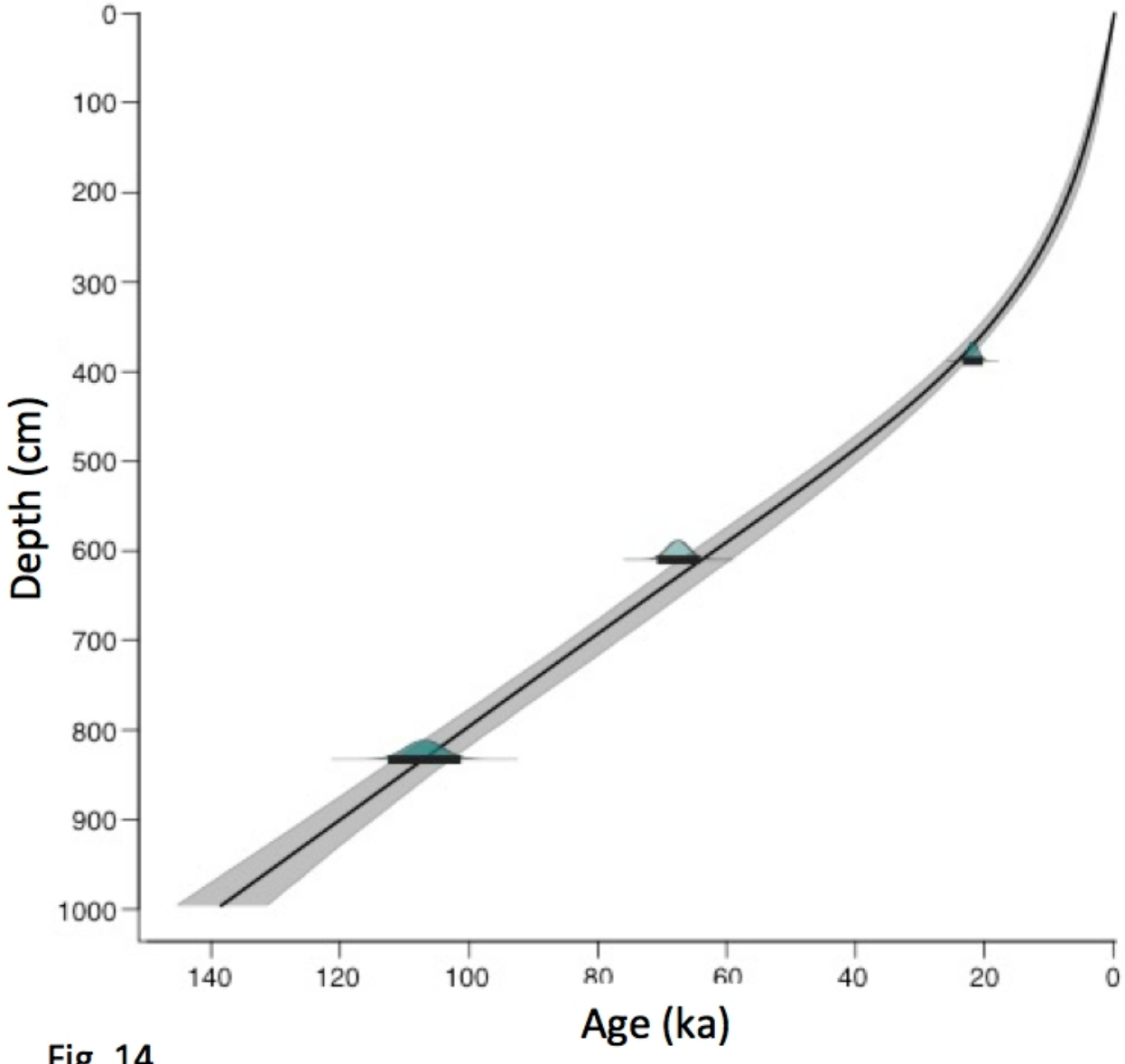
Depth (cm)
0
100
200
300
400
500
600
700
800
900
1000
140
120
100
80
60
40
20
0
Age (ka)

Fig. 14

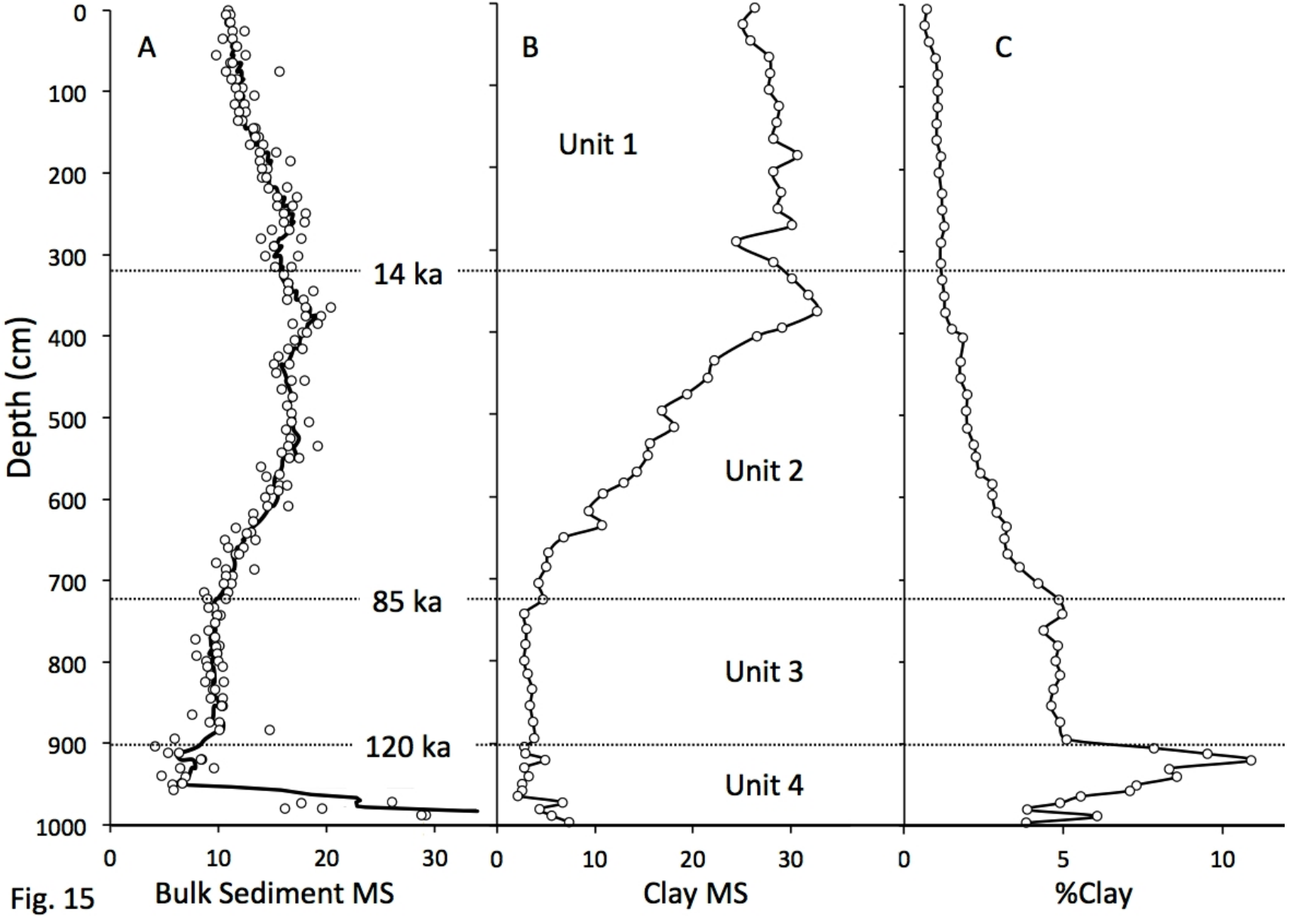
A
B
C
Unit 1
Unit 2
Unit 3
Unit 4
14 ka
85 ka
120 ka
Depth (cm)
0
100
200
300
400
500
600
700
800
900
1000
0
10
20
30
Bulk Sediment MS
Clay MS
%Clay
5

Fig. 15

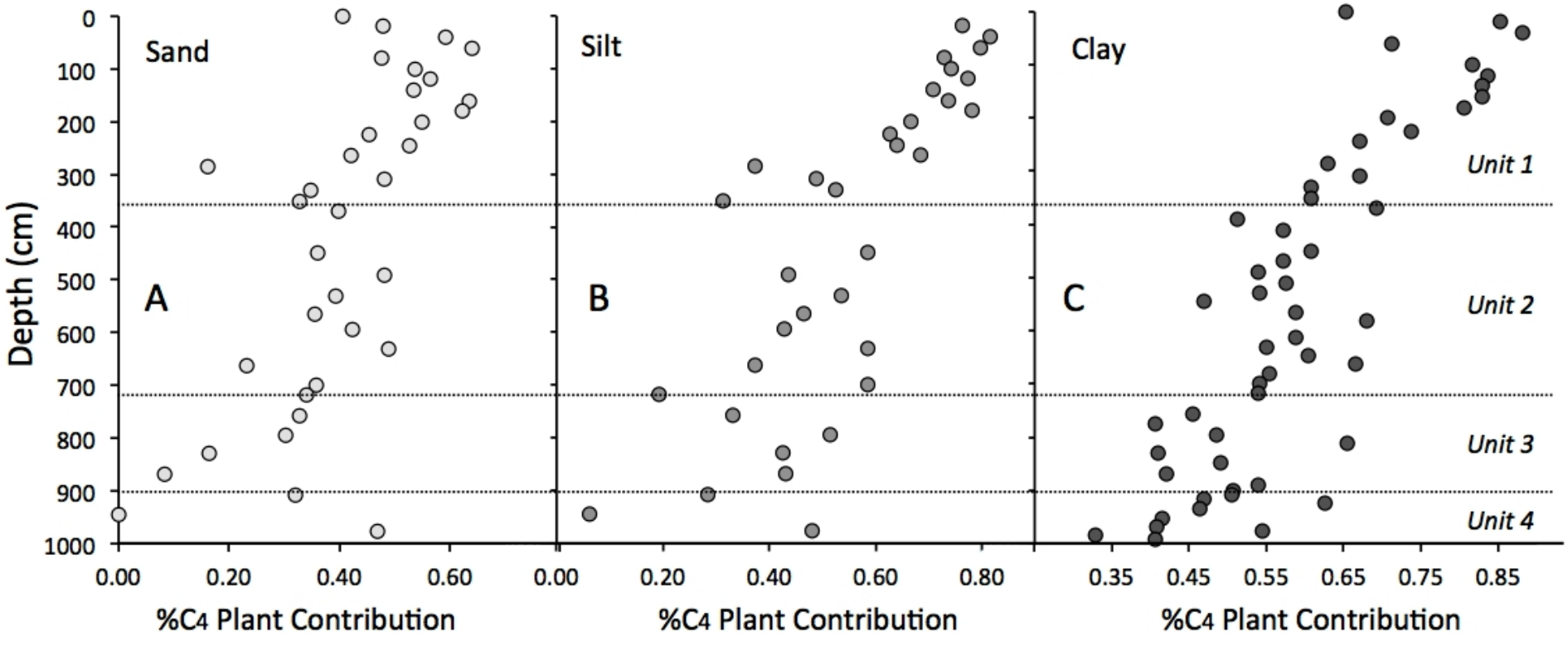
Sand
Silt
Clay
A
B
C
Unit 1
Unit 2
Unit 3
Unit 4
Depth (cm)
0
100
200
300
400
500
600
700
800
900
1000
0.00
0.20
0.40
0.60
0.00
0.20
0.40
0.60
0.80
0.35
0.45
0.55
0.65
0.75
0.85
%C4 Plant Contribution
%C4 Plant Contribution
%C4 Plant Contribution

Fig. 16

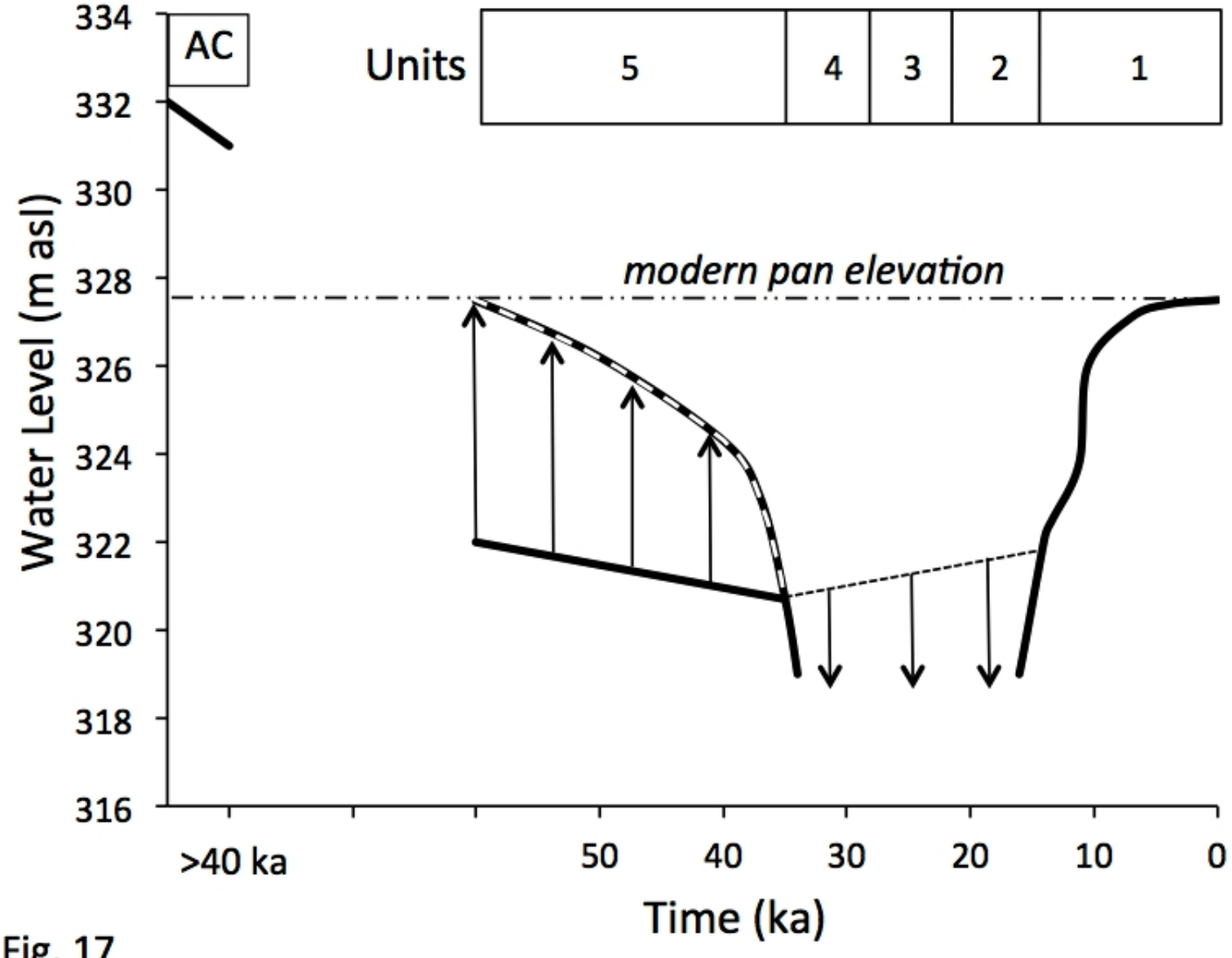
AC
Units
5
4
3
2
1
modern pan elevation
Water Level (m asl)
334
332
330
328
326
324
322
320
318
316
>40 ka
50
40
30
20
10
0
Time (ka)

Fig. 17

Miller et al. WCC
Figure Captions

Fig. 1 Median January-March rainfall over mainland Australia with the locations of Wolfe Creek Crater (WCC), Halls Creek (HC) and Sturt Creek Station (SC). Figure from Australian Bureau of Meteorology based on 1960-1990 data.

Fig 2 Satellite image of Wolfe Creek Crater (WCC), longitudinal dunes, and Wolfe Creek at the far left. Source: Google Earth.

Fig. 3 Halls Creek 9 AM windrose; velocities in km hr^{-1}. Figure from Australian Bureau of Meteorology based on 6000 observations.

Fig. 4 Satellite image of Wolfe Creek Crater showing the disruption caused by a meteorite impact close to the center of an established E-W trending longitudinal dune. Formation of the crater wall deflected prevailing easterly winds, resulting in a new, horseshoe-shaped dune wrapping around the crater. ASTER VNIR image (bands 3, 2 and 1) taken 02-02-2003 (Wright et al., 2013)

Fig. 5 Dormer auger system with "Jarret" style auger head (a) and OSL sediment "shaver" (e) used to prepare sediment in the hole for OSL sampling. The rod to which stainless steel OSL sample tube is attached (g) is driven into the sediment with a small sledgehammer. From Munyikea et al. (2011).

Fig. 6 Vertical image of Wolfe Creek Crater with the primary sample sites located.

Fig. 7 East-West surveyed cross section through the crater showing the flat central pan, offset somewhat to the east of the actual center of the crater. Exaggerated vertical scale of the inset figure provides scaled auger holes and reconstructed facies changes documenting the lack of a U-shaped central crater pan before gypsum precipitates flattened the central region. Initial gypsum precipitates expanded outward in the early Holocene, expanding the area covered by a flat pan, but contracted in the late Holocene as alluvial processes delivered more sediment from the crater walls to the alluvial fans that have been expanding through the late Holocene, diminishing the area occupied by the central pan.

Fig. 8 Oblique aerial view of Wolfe Creek Crater looking SE, showing the northern arm of the horseshoe dune created by the crater's impact on aeolian sand transport, and the location of augered holes 01WCC-13 and 01WCC -14. Photo credit: GHM

Fig. 9 Surveyed profile across the northern horseshoe dune showing the augered hole that reached intact ferricrete and ~10 m depth. The lowest meter consists of sand mixed with small fragments of ferricrete interpreted to be primary impact debris.

Fig. 10 Surveyed profile eastward from the highest point on the eastern crater rim showing the locations of four of the augered holes (dark vertical lines) that document the

thickness of the aeolian sand wedge (stippled) that overlies bedrock rubble ejected from the crater on impact at shallow depths (3 to 4 m). The approximate surface of the western crater wall is shown as a dotted line for comparison.

Fig. 11 Primary core log for WCC99-04, bulk sediment magnetic susceptibility, radiocarbon and OSL dates, and derived stratigraphic units. Boxes indicate location of biosilicate samples.

Fig. 12 Bulk sediment $\delta^{13}C$ values (A), percent organic carbon (B), and hygroscopic moisture in bulk sediment (CC) from WCC99-04. Mean and standard deviations are shown from most intervals, stippled where the central tendency is tightly constrained.

Fig. 13 Iron, magnesium and aluminum oxides in bulk sediment from nine levels through WCC99-04, show systematic changes in composition through the primary sedimentary units. Oxides were measured by ICP-MS.

Fig. 14 Age model for 01WCC-13 based on 3 OSL dates through the hole, and assuming a surface age of modern, derived by fitting a smoothed spline through the OSL dates using CLAM (Blaauw, 2010). The derived ages for the boundaries of sedimentary units are given in Figure 15.

Fig. 15 Bulk sediment MS (A), clay MS (B), and percent clay (C) in 01WCC-13, showing derived sedimentary units with boundary ages from Figure 14.

Fig. 16 Sedimentary organic matter $\delta^{13}C$ values in sand, silt and clay fractions from 01WCC-13, with unit boundaries derived from changes in sediment physical characteristics (Fig. 15) superimposed. Isotopic values have been converted to %C4 plant contribution as described in Section 8.4

Fig. 17 Lower portion: Reconstructed changes in Wolfe Creek Crater water-table level based on characteristics of sediment in the central crater pan back to ~60 ka (WCC99-04). Solid line is always the minimum water table required, whereas the dashed line is an estimate of actual water table, when likely much above the minimum level. The maximum lowering of the water table between 35 and 14 ka remains unconstrained, but changes in the sediment character suggest the water table was rising before 14 ka. An older, high water level is based on algal carbonates (AC). The positions of WCC99-04 stratigraphic units (Fig. 11) on which the water-table is based, are indicated in the closed boxes.